

Thesis report

Modelling Differential Diffusion in Turbulent Non-Premixed Hydrogen Flames

M.M. Nelissen

P&E report number 3040



Thesis report

Modelling Differential Diffusion in Turbulent Non-Premixed Hydrogen Flames

by

M.M. Nelissen

to obtain the degree of Master of Science
at the Delft University of Technology.
to be defended publicly on Thursday January 7, 2021 at 09:30 AM.

Student number: 4278542
Thesis committee: Prof. dr. D.J.E.M. Roekaerts TU Delft, supervisor
Prof. dr. ir. S. Klein, TU Delft
Dr. I. Langella, TU Delft

An electronic version of this thesis is available at <http://repository.tudelft.nl/>.

Abstract

In the future, fossil fuels will be replaced by renewable sources. Hydrogen seems to be a promising energy carrier (fuel). A lot of research has been conducted on the combustion of hydrogen, but the effect of the high diffusivity of hydrogen compared to other species (differential diffusion) was often not included in simulations of turbulent flames because turbulent mixing is expected to suppress strong influence of differential diffusion. Nevertheless effects of differential diffusion have been reported in experiments. The main purpose of this thesis is to include the effect of differential diffusion in a CFD model of turbulent non-premixed hydrogen flames and to validate the models with available experimental data. The validation data set used in this study is a non-premixed turbulent jet flame of hydrogen diluted with nitrogen on 50/50 volume ratio. This flame is interesting because the role of differential diffusion in this flame has been a matter of discussion in the literature.

A review is given of previous work on turbulent non-premixed hydrogen flames and effects of differential diffusion. It is concluded that the Flamelet Generated Manifold (FGM) model and the Transported Probability Density Function (PDF) model are both promising turbulent combustion models for these flames. Next, a new comparative study is made of several turbulence and combustion models using Reynolds-averaged Navier Stokes simulations in Ansys Fluent, and focusing on FGM as turbulent combustion model. It is concluded that the standard $k - \epsilon$ with a correction as suggested by Pope is the best choice for the turbulence model. The ANSYS Fluent implementation of FGM does not have the option to include differential diffusion. Therefore it is added in a separate way. To do this, flamelets are created with the help of CHEM1D, a tool developed by TU Eindhoven. These flamelets are combined to an FGM table also including the effect of turbulence via a PDF and this table is imported into Fluent with the help of a user-defined function overwriting the default Fluent FGM table.

In order to clearly see the effects of differential diffusion, simulations with and without differential diffusion are made. Good agreement is obtained between experimental results and the numerical simulation for the models without differential diffusion. This confirms that turbulence can suppress strong influence of differential diffusion. In experiments effects of differential diffusion have been observed at the base of the flame, close to the burner nozzle. The model simulations with differential diffusion included, provide a slightly more accurate prediction of the mean temperature close to the nozzle but still large discrepancies remain.

Acknowledgements

Throughout my studies at the TU Delft, and especially while writing this thesis, I have received a great deal of support and assistance, for which I would like to thank the following people.

Firstly I would like to express my gratitude to my supervisor Prof. Dr. Dirk Roekaerts. His guidance, support and feedback helped greatly towards finishing this project. He devoted a lot of his time to this work, including but definitely not limited to explaining concepts in depth and writing one of the Appendices in this report. I would also like to thank Mengmeng Ren, Naiara Romero-Anton and Jeroen van Oijen. Their research and insights have been pivotal for this work. Furthermore I would like to thank my examination committee for their time and effort examining this thesis.

Finally I would like to thank my parents, friends and especially my boyfriend for their encouragement and support. Staying focused and motivated would not have been possible without their help, especially during these unprecedented times.

*M.M. Nelissen
Rijswijk, December 2020*

Contents

Abstract	iii
Acknowledgements	v
Nomenclature	ix
List of Figures	xi
List of Tables	xiii
1 Introduction	1
1.1 Motivation	1
1.2 Research Questions	1
1.3 Thesis Outline	2
2 Literature Review	3
2.1 H3 Flame	3
2.1.1 Measurements	3
2.1.2 Past Research	4
2.2 Differential Diffusion	6
2.2.1 Definition and Relevance	6
2.2.2 Recreating the H3 Graphs	8
2.2.3 Past Research	8
3 Computational Models	11
3.1 Chemical Model	11
3.2 Turbulence Model	12
3.2.1 $k-\varepsilon$ Model	12
3.2.2 Reynold Stress Model	13
3.3 Combustion Model	13
3.3.1 Transported PDF Model	13
3.3.2 Flamelet Generated Manifold Model	14
3.4 Model Choices	15
3.4.1 UDF with CHEM1D	16
4 Results and Discussion	17
4.1 CHEM1D	17
4.1.1 Setup of CHEM1D	17
4.1.2 Results of CHEM1D compared to Data	17
4.2 Turbulent Flame Simulation	20
4.2.1 Case Description	20
4.2.2 Mesh Setup	20
4.2.3 Boundary Conditions	22
4.2.4 Models	23
4.3 Chemical Equilibrium Model	24
4.4 Other Fluent Models	26
4.4.1 Steady Diffusion Model	26
4.4.2 FGM Model	27
4.5 Flamelet Generated Manifold model with UDF	28
4.5.1 Unity Lewis Numbers	28
4.5.2 Non-unity Lewis Numbers	29
4.5.3 Sensitivity to Chemical Model	32

4.6 Model Comparison	33
4.7 Comparison to previous research	36
4.8 Statistical Dependence	39
5 Conclusions and Recommendations	41
A UDF code	43
B Relation between variance of unscaled and scaled progress variable	55
Bibliography	57

Nomenclature

Symbols

α	Thermal diffusivity	m^2/s
α_k	Constant in progress variable definition	
χ_c	Scalar dissipation rate	$1/\text{s}$
$\dot{\omega}$	Species mass reaction rate	$\text{kg}/\text{m}^3\text{s}$
$\dot{\omega}_c$	Progress variable source term	$1/\text{s}$
λ	Thermal conductivity	$\text{W}/\text{m K}$
μ_t	Turbulent viscosity	$\text{N}/(\text{m}^2 \text{s})$
ϕ	Mass flux density	$\text{kg}/\text{m}^2\text{s}$
ψ	Composition space vector	
ρ	Density	kg/m^3
τ_{ij}	Viscous stress tensor	N/m^2
ε	Turbulent dissipation rate	m^2/s^3
k	Turbulent kinetic energy	m^2/s^2
c	Reaction progress variable	
c_p	Specific heat	$\text{J}/\text{kg K}$
D	Mass diffusivity	m^2/s
F_{kj}	Turbulent scalar flux	
g	Gravitational acceleration	m/s^2
G_k	Function of stress tensor	
h	Enthalpy	J
J	Diffusion flux	$\text{kg}/\text{m}^2\text{s}$
Le	Lewis number	
M	Molar mass	kg/Mole
P	Favre joint PDF	
R_{ij}	Reynolds stress tensor	N/m^2
S_k	Reaction rate of species k	Mole/s
S_k	Source term	
T	Temperature	K
t	Time	s

u_i''	Fluid velocity fluctuation vector	m/s
u_i	Favre mean fluid velocity vector	m/s
v	Velocity	m/s
w	mass	kg
x	spatial coordinate	m
Y_k	Species mass fraction	
Z	Mixture fraction	

Subscripts

b	burnt state
eq	Chemical equilibrium
i,j,k	species/element number
i,j,k	x,y and z direction
u	unburnt state

Abbreviations

BC	Boundary Condition
CE	Chemical Equilibrium
CFD	Computational Fluid Dynamics
CMC	Conditional Moment Closure
DD	Differential Diffusion
DNS	Direct Numerical Simulation
EDC	Eddy Dissipation Concept
EDM	Eddy Dissipation Model
EMST	Euclidian Minimum Spanning Tree
FGM	Flamelet Generated Manifold
IEM	Interaction by Exchange with the Mean
LES	Large Eddy Simulation
ODT	One Dimensional Turbulence
PDF	Probability Density Function
PV	Progress Variable
RANS	Reynolds Averaged Navier Stokes
RSM	Reynold Stress Model
T-PDF	Transported Probability Density Function
TKE	Turbulent Kinetic Energy
UDF	User Defined Function

List of Figures

2.1	Sketch of the setup of the H3 flame	3
2.2	Test setup of the H3 flame [25]	4
2.3	Results from D'Ausilio regarding the temperature at the radial profile [13]	6
2.4	Temperature vs mixture fraction in comparison to adiabatic equilibrium. F_o is the mixture fraction based on element O and f_H is the mixture fraction based on element H. [25]	7
2.5	Temperature vs mixture fraction in comparison to adiabatic equilibrium at $x/d=2.5$. F_o is the mixture fraction based on element O and f_H is the mixture fraction based on element H.	9
3.1	Schematic overview of modelling approaches for turbulent combustion (adapted from Perpignan et al. [31])	11
4.1	Temperature vs Progress variable for the data (left) and CHEM1D (right), where the color represents the mixture fraction	18
4.2	Mass fraction of hydrogen element vs mixture fraction for the data (left) and CHEM1D (right), where the color represents the progress variable	18
4.3	Mass fraction of oxygen element vs mixture fraction for the data (left) and CHEM1D (right), where the color represents the progress variable	19
4.4	Progress variable vs mixture fraction for the data (left) and CHEM1D (right)	19
4.5	Progress variable vs mixture fraction for CHEM1D with and without unity Lewis numbers and the Data	20
4.6	Temperature vs mixture fraction based on hydrogen element (left) and oxygen element (right)	20
4.7	Setup of the H3 flame	21
4.8	Temperature profiles for different meshes at $x/D=2.5$, using the chemical equilibrium model with the Li mechanism	21
4.9	Temperature profiles for different meshes at $x/D=20$, using the chemical equilibrium model with the Li mechanism	21
4.10	Overview of whole domain with fine mesh	22
4.11	Mesh layout for both the fine mesh (left) and the very fine mesh (right)	22
4.12	Overview of boundaries. Blue = inlet, Red = outlet, Yellow = symmetry and Black = wall.	22
4.13	Turbulent kinetic energy and velocity along the centerline for various turbulent intensities (TI) using the chemical equilibrium model with the Li mechanism	23
4.14	TKE and velocity along the centerline for standard and adapted standard $k-\epsilon$ model	24
4.15	TKE and velocity along the centerline for realizable and adapted realizable $k-\epsilon$ model	25
4.16	Radial velocity profiles at various locations	26
4.17	Major species along the centerline	26
4.18	Radial profiles of mixture fraction (left) and temperature (right) at various locations	26
4.19	Mixture fraction (left) and temperature (right) along the centerline	26
4.20	TKE and velocity along the centerline for steady flamelet model (left) and standard FGM model (right)	27
4.21	Radial velocity profiles at various locations for steady flamelet model (left) and standard FGM model (right)	27
4.22	Major species along the centerline for steady flamelet model (left) and standard FGM model (right)	28
4.23	(Un-normalized) Progress Variable at different positions (left) and along the centerline (right).	29
4.24	Temperature at different positions (left) and along the centerline (right)	29
4.25	Un-normalized Progress Variable variance contour with a super imposed line at $x/d=20$	30
4.26	Contour of the velocity (left) and the temperature (right)	30
4.27	Un-normalized Progress Variable at different positions (left) and along the centerline (right).	31
4.28	Temperature at different positions (left) and along the centerline (right)	31

4.29	Progress variable vs mixture fraction where the color represents the progress variable source term. Mechanisms used are by Li et al. [22] with DD (top left), Li et al. without DD (top right), Burke et al. [6] with DD (bottom left) and a mechanism by ELTE with DD [27] (bottom right) . . .	32
4.30	Comparison of the Li mechanism and the Burke mechanism for the temperature at various positions (left) and along the centerline (right)	33
4.31	Source term of PV vs temperature for 2 different PDF integrated tables	34
4.32	Mixture fraction vs temperature (left) and mixture fraction vs source term of PV (right) for 2 different PDF integrated tables	34
4.33	Velocity (left) and mixture fraction (right) at different positions. Black is measured at $x/d=5$ (velocity) and $x/d=2.5$ (FBLGR), red is measured at $x/d=20$ and green is measured at $x/d=20$. . .	35
4.34	Temperature at $x/d=2.5$ (left) and at $x/d=20$ (red) and $x/d=40$ (green) (right)	35
4.35	Un-normalized progress variable at different positions (left) and along the centerline (right) . . .	35
4.36	Mixture fraction (left) and temperature (right) at various locations by D'Ausilio et al. [13]	37
4.37	Temperature at $x/d=5$ (left) and $x/d=20$ (right) where the symbols are experimental data, the solid lines include differential diffusion and the dotted lines do not, by Maragkos et al. [24] . . .	37
4.38	Temperature along the centerline by Pitsch et al. [34]	37
4.39	Scaled Progress variable vs mixture fraction for a data points at $x/d=10$	40
4.40	Comparison of marginal PDF and β -PDF for the mixture fraction (left) and scaled progress variable (right) at $x/d=10$	40

List of Tables

3.1	Values of empirical constants in $k - \epsilon$ model as proposed by Poinso et al. [35]	12
3.2	Non-premixed combustion models included in Ansys Fluent and their properties	13
4.1	Error analysis of velocity and k along the centerline	25
4.2	Overview of FGM methods used	28
4.3	Error analysis of maximum flame temperature	34
4.4	Error analysis of maximum flame temperature location	34
4.5	Key characteristics of four simulations	38

1

Introduction

This chapter contains a short motivation on the relevance of this work. Research questions are formulated and the thesis outline is discussed.

1.1. Motivation

Looking at the future of energy it is clear that the use of fossil fuels should be reduced massively in order to reduce emissions and stop global warming. Initiatives such as the Paris agreement set goals for the future in terms of greenhouse gas emission mitigation. In the Netherlands the National Climate Agreement was set-up recently as a part of the Dutch climate policy. It contains the plans which the Dutch government wants to execute in order to reduce the greenhouse gas emissions. Several steps can be taken to achieve this, and one is to eliminate/reduce the use of fossil fuel and get electricity from renewables such as wind, solar and biomass. Not all of the fossil fuels can be replaced by electricity and need combustible fuel. This is where hydrogen comes in. Hydrogen seems to be a promising energy carrier [16], as its emissions are very low. A lot of research is conducted with respect to the use of hydrogen as fuel in turbomachinery, either diluted or pure. Flashback is a large problem when it comes to the combustion of hydrogen but other phenomena need to be modelled correctly as well in order to get a reliable model. One of these phenomena is differential diffusion. Usually in a turbulent model, it is assumed that all species have the same diffusivities. This assumption cannot be made when one wants a high accuracy in calculations, or when one of the species has a diffusivity which is much larger or smaller than the other ones. Taking these different diffusivities into account is also known as differential diffusion. Differential diffusion occurs in both premixed and non-premixed flames, and is still a widely researched topic. Differential diffusion influences the laminar flame speed, which can be underpredicted if it is not included. This is important for the modelling of flashback. Even though premixed flames are usually used in the industry, it is still valuable to research non-premixed flames to get a better understanding of hydrogen and the modelling techniques. The H3 flame is a well-known benchmark flame and is very suitable for research regarding differential diffusion. From past research (Chapter 2) it can be seen that differential diffusion is dominant close to the nozzle, but was almost never researched. Maragkos [24] included the effect of differential diffusion but used a very simple chemical scheme. His research can therefore still be improved by using a more elaborate chemical scheme. For this thesis, it is proposed to model differential diffusion in the H3 flame, including an appropriate chemical scheme.

1.2. Research Questions

The aim of this thesis is to make a RANS simulation of differential diffusion using the H3 flame. It is preferred to use Ansys Fluent as the CFD software. The data from the H3 flame will be used to validate the model. The following research questions will formulate the goal of this thesis:

- Is it possible to include differential diffusion in a RANS model in ANSYS?
- What computational models should be used to get the most accurate results?

- Does using a more elaborate chemical scheme result in better results (compared to Maragkos [24])?
- Do the flame temperature and gas composition predictions improve in the simulation when including differential diffusion?

1.3. Thesis Outline

Chapter 2 contains a literature review which summarizes the most relevant research done with respect to the H3 flame and differential diffusion. The theory of differential diffusion is introduced and several models that can be used to simulate this effect are obtained. Chapter 3 explains more about the computational models that are considered. The chemical, turbulence and combustion models are discussed including methods to include these models in Fluent. Chapter 4 presents the results of several different simulations done in this work which are analyzed and compared to each other and to previous research. Finally, Chapter 5 contains a summary of the conclusions of this work and recommendations for future research that resulted from these conclusions.

2

Literature Review

This chapter will discuss previous research in the field of turbulent diffusion flames and differential diffusion.

2.1. H3 Flame

The H3 flame is a flame which has been used as a standard benchmark case since 1996 [21]. A sketch of the flame setup is shown in Figure 2.1. It was investigated at the TU Darmstadt. The fuel consists of hydrogen which is diluted by nitrogen in a 50/50 ratio. The nitrogen dilute was used in order to reduce the heat loss by radiation which will simplify the simulations [25]. The fuel jet has a velocity of 34.8 m/s and a Reynolds number of 10,000. Experimental data of this flame can also be found on the website of the DLR. [21]. It is said that the flame was first used to research the modelling of turbulent flames because of its simple composition, once the modelling was successful natural gas could be studied. Nowadays the flame is interesting as society is looking into the combustion of hydrogen in order to lower greenhouse gases. Information on the measurements and research conducted using the H3 flame will be summarized below.

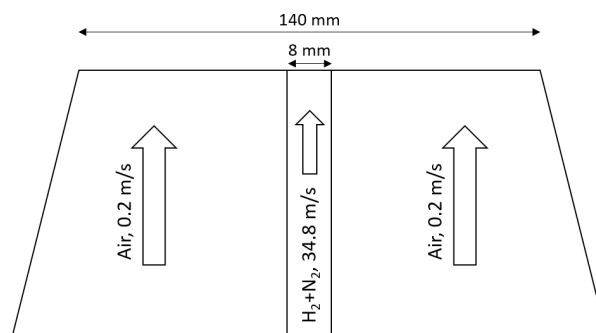


Figure 2.1: Sketch of the setup of the H3 flame

2.1.1. Measurements

The first measurements of the H3 flame were done by Meier et al. [25]. A large data-set was created which will be used in this thesis as validation. The obtained data consists of 300 single-shots at 249 locations and provides the temperature, the Bilger mixture fraction and mass fractions of the main species (O_2 , H_2 , H_2O and N_2). The radial sections used are $x/d=2.5, 10, 20, 30, 40, 50$ and 70 . As physical sensors usually cause perturbations in flames it was desired to use a laser-based technique to get the most accurate results. Meier et al. therefore decided to use single-shot Raman scattering. The setup of the Raman Scattering is shown in Figure 2.2. This setup uses a flashlamp-pumped dye laser to measure species concentrations and temperature simultaneously at a certain point in time. The measurements were deemed of high accuracy, 3% for the temperature and 3-5% for the concentrations for single pulse measurements.

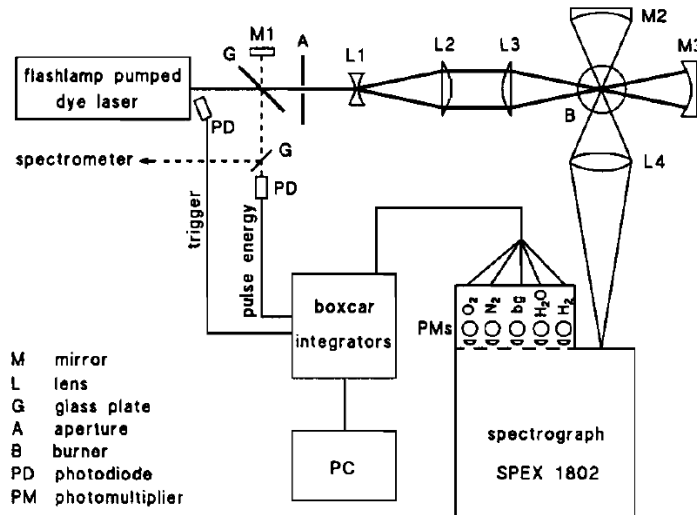


Figure 2.2: Test setup of the H3 flame [25]

In addition to the measurements made by Meier et al, Pfuderer et al. [32] did measurements in order to validate their turbulent model. They measured the velocity using a 3D Laser-Doppler Velocimetry system. Like the Raman scattering this technique uses lasers to do measurements as they do not disturb the flame and influence the results. Once again this technique was deemed of high accuracy, errors are typically 2% to 5% in mean velocities [12]. The velocity was obtained at 19 points in cross-sections $x/d=5, 20, 40, 60$ and 80 . Each point provides information on $u, v, w, u'u', v'v', w'w', u'v'$ and $u'w'$. here $u, v,$ and w are the velocities in the x, y and z direction and the other variables are variances on the velocity.

2.1.2. Past Research

In 1996, Meier et al. [25] measured mass fractions of species and the temperature. Using the obtained data Meier shows that differential diffusion has a significant influence on the H3 flame close to the exit of the fuel pipe, but the effect diminishes further downstream. The first researchers to use the H3 flame in order to validate a turbulent model were Pfuderer et al. [32]. They made a Reynolds-averaged Navier Stokes (RANS) model and tried to include the effect of differential diffusion. The two chemical models that were considered were the chemical equilibrium approach and laminar flamelet approach. Due to limitations in the laminar flamelet approach, the chemical equilibrium approach was used as it would give better results. The overall correlation between the model and the data is satisfactory.

Neuber et al. [29] wanted to predict the mole fractions of NO and OH. The effect of differential diffusion was not included, hence it was chosen to have the lowest measured cross-section at $x/d=20$ to get accurate results. Using a presumed β -Probability Density Function (PDF), $k-\epsilon$ turbulent model and a system of 7 reactions, a model was build. The major species were predicted quite well. Even though presumed PDF cannot predict the minor species sufficiently, it was still considered a good estimation, especially considering the measurement error that the minor species can have.

Pitsch et al. [34] also used H3 as a validation for their model. They wanted to model turbulent hydrogen-air flames using the unsteady flamelet model. Their approach used three different combustion models: the steady flamelet library without radiation, the first model but using the results to predict the unsteady flamelet and an unsteady flamelet. Differential diffusion was not included in these calculations. They concluded that a steady flamelet cannot predict NO formation and that radiation is not important for the general flame structure.

The next research using the H3 flame was done by Forkel et al. [17]. They tried to use Large Eddy Simulation (LES) instead of RANS. The emphasis was put on the boundary conditions at the inlet. Two different sets

of boundary conditions were used: coupled and random. Coupled uses fully developed turbulent pipe flow and random used random forcing with mean profiles identical to the coupled one. The random B.C. was not very successful as the random noise was too different from the real turbulence. The coupled B.C. gave better results but is also not perfect.

Echekki et al. [15] used the One-Dimensional Turbulence (ODT) model to simulate the turbulent flame. It has a good description of the coupling of turbulence and chemistry with an additional advantage when it comes to computational cost, but its applications are limited due to the low dimensional nature. Echekki combined the ODT model with a five-step chemistry model to simulate the behaviour of H3. ODT gives relatively good predictions but when flows get more complex, another model has to be used. When it comes to differential diffusion, the results show that differential diffusion occurs, even though it is not a very accurate representation.

In 2002, Kempf et al. [20] made a LES model and focused on the chemistry effects. The goal of their research was to see how LES can improve the modelling of turbulent combustion with respect to RANS. Thermochemistry was described by a steady flamelet model and the LES subgrid model is the Smagorinsky model. Although the model is quite accurate, it cannot describe differential diffusion, even though differential diffusion is relevant in this case. Renfro et al. [40] used H3 to compare OH time series measurements and Ranganath et al. [38] used it as a reference for another ODT model. Both of them did not take differential diffusion into account.

Maragkos et al. [24] were the first to try and include differential diffusion in their model, almost 20 years after it was stated by Meier [25] that differential diffusion had a large influence on the H3 flame. The goals of their research were to extend the methodology from a previous research on laminar flames to include differential diffusion and to quantify whether differential diffusion has a significant effect in turbulent combustion. They used an LES model in OpenFOAM which uses presumed β -PDF as turbulence chemistry model and one step Burke-Schuman as the chemical model. It was found that the inclusion of differential diffusion had an influence on the maximum flame temperature and on the stabilization and position of the flame. The results obtained are in good agreement with the experimental data, but there is some improvement needed when it comes to the inlet boundary condition. The B.C. which is used at the inlet (velocity 'white noise') is known to be an inaccurate representation of turbulence. Maragkos states that the combustion model used is relatively simple and that it would be interesting to examine the influence and accuracy of this model when compared to other models.

The most recent research regarding H3 has been conducted by D'Ausilio et al. [13]. A LES model was set up using the Conditional Moment Closure model (CMC) as combustion model. It was paired with the reaction mechanism presented by Li et al. [22]. The focus of the research was on the inlet boundary condition and on differential diffusion. The inlet boundary condition that was proposed was the random spots methods, which is "based on the idea that turbulent flow is a motion of turbulent spots of a certain size arising at random positions at random times". In the model, turbulence decays unrealistically near the nozzle, which is most likely due to the random spots method. It was therefore concluded that this B.C. is limited but can still be a good choice depending on the goal of the research as it lowers computational cost. Differential diffusion was not included in the model, but its importance and influence on the flame was analysed in the research as it cannot be neglected. It was concluded that differential diffusion has effect close to the nozzle but the effect vanishes further downstream when transport by turbulence dominates. This effect can be seen in Figure 2.3, as the difference in temperature between experiment and model at $x/d=5$ can be explained by the fact that differential diffusion is present but not modelled.

Summarizing the research that has been conducted on H3 shows that differential diffusion is important but has only been acknowledged by few and implemented by only one. This is probably due to the fact that H3 is considered as a simple benchmark case and a lot of the research conducted uses this flame as a first estimate and moves on to other, more complicated fuels once the results are satisfactory. This usually makes the differential diffusion effect negligible as it occurs due to the fact that hydrogen has a very large diffusion coefficient. In the current climate however, hydrogen is considered as a replacement for fossil fuels [16] and hence it is important to research it as much as possible. Understanding and modelling differential diffusion can help to obtain better predictions of the flame temperature and NO_x emissions.

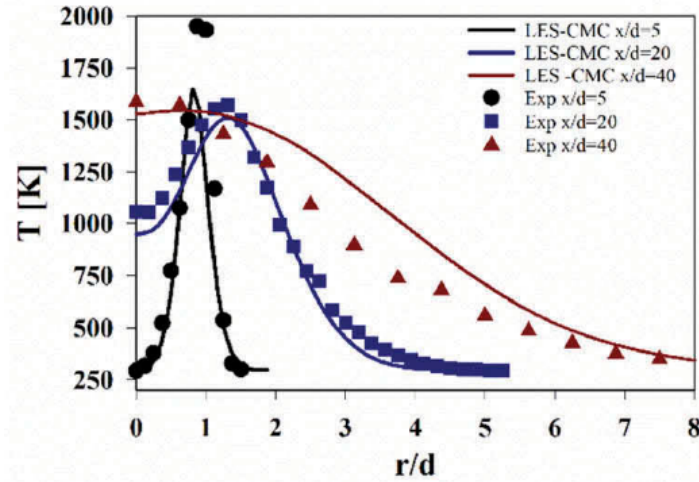


Figure 2.3: Results from D'Ausilio regarding the temperature at the radial profile [13]

2.2. Differential Diffusion

The modelling of differential diffusion has also been researched quite extensively. A quick overview of differential diffusion and a summary of papers on modelling this effect will be summarized here. The focus will be on research that used hydrogen flames and computational models that are compatible for RANS simulations, but some research using other models is included as well.

2.2.1. Definition and Relevance

Information in this section has been obtained from d'Ausilio et al. [13], Meier et al. [26], Gao et al. [18], Warnatz et al. [45] and the lectures of the AE4262 course at the TU Delft.

In a mixture, different species all have their own diffusivities. The Lewis number is usually used as a non-dimensional number to express diffusivity. It is shown in Equation 2.1 and can be described as the ratio of the thermal diffusivity (α) to mass diffusivity (D). In turbulent combustion, it is assumed that the diffusivity of all the molecules is equal (or that the Lewis number equals unity). This based on the assumption that turbulent mixing is more dominant than molecular mixing. This assumption does not hold when a fast diffusing species such as hydrogen is involved (which has a Lewis number of about 0.2). Especially close to the nozzle, molecular diffusion will be more dominant than turbulent mixing and therefore the assumption of equal diffusivities does not hold. Including the different diffusivities is also known as differential diffusion (or in some cases as molecular diffusion). In the case of laminar premixed flames, the flame speed can be inaccurate when excluding differential diffusion. For the H3 flame (which will be used in this thesis), it is stated by Meier that not including differential diffusion can have an effect on the modelling of flame temperature and gas composition.

$$Le = \frac{\alpha}{D} \quad (2.1)$$

In order to show that differential diffusion does indeed occur, one can plot various graphs. One way is to plot the mixture fraction vs temperature, where a mixture can be compared to the adiabatic equilibrium. In Figure 2.4 the temperature vs mixture fraction of the H3 flame is shown, including the adiabatic equilibrium. In the case of very fast reactions and equal diffusivities the adiabatic equilibrium temperature is realized. In the two plots at $x/d=2.5$ it can be seen that there is a temperature increase above the adiabatic temperature. This is due to the fact that the Lewis number is less than unity, meaning that the mass diffusion rate is higher than the heat diffusion rate. In the case of a non-unity Lewis number, differential diffusion occurs.

Since differential diffusion is present in H3, it should be included in a model. Several methods can be applied to reduce computational time, but this often means that differential diffusion is not included due to these simplifications. The first method is the use of a Reynolds-averaged Navier-Stokes (RANS) approach. There are

several terms in the transport equations that need to be closed. The RANS equations are shown in equations 2.2, 2.3 and 2.4. When modelling a flow there are usually terms that cannot be closed due to nonlinear terms in the equations. In the case of a RANS approach the unclosed terms are the Reynolds stress ($-\bar{\rho}\tilde{R}_{ij}$), turbulent scalar flux ($-\bar{\rho}\tilde{F}_{kj}$) and the mean source term ($\bar{\rho}\tilde{S}_k$). The mean source term will be the hardest to close. Usually laminar transport is small compared to turbulent transport, which means $\bar{J}_{k,i} \ll \bar{\rho}\tilde{F}_{k,i}$. Therefore $\bar{J}_{k,i}$ is often neglected, but when the Reynolds number is low or when differential diffusion effects are strong it cannot be neglected. Differential diffusion can influence the local flame structure and therefore can play a role in the closure of the mean source term.

$$\frac{\partial}{\partial t}(\bar{\rho}) + \frac{\partial}{\partial x_i}(\bar{\rho}\tilde{v}_i) = 0 \quad (2.2)$$

$$\frac{\partial}{\partial t}(\bar{\rho}\tilde{v}_j) + \frac{\partial}{\partial x_i}(\bar{\rho}\tilde{v}_i\tilde{v}_j) = \left[-\frac{\partial\bar{p}}{\partial x_j} + \frac{\partial\bar{\tau}_{ij}}{\partial x_i} + \bar{\rho}g_j \right] - \frac{\partial}{\partial x_i}(\bar{\rho}\tilde{R}_{ij}) \quad (2.3)$$

$$\frac{\partial}{\partial t}(\bar{\rho}\tilde{\phi}_k) + \frac{\partial}{\partial x_i}(\bar{\rho}\tilde{\phi}_k\tilde{v}_i) = \left[-\frac{\partial}{\partial x_i}(\bar{J}_{k,i}) + \bar{\rho}\tilde{S}_k \right] - \frac{\partial}{\partial x_i}(\bar{\rho}\tilde{F}_{kj}) \quad (2.4)$$

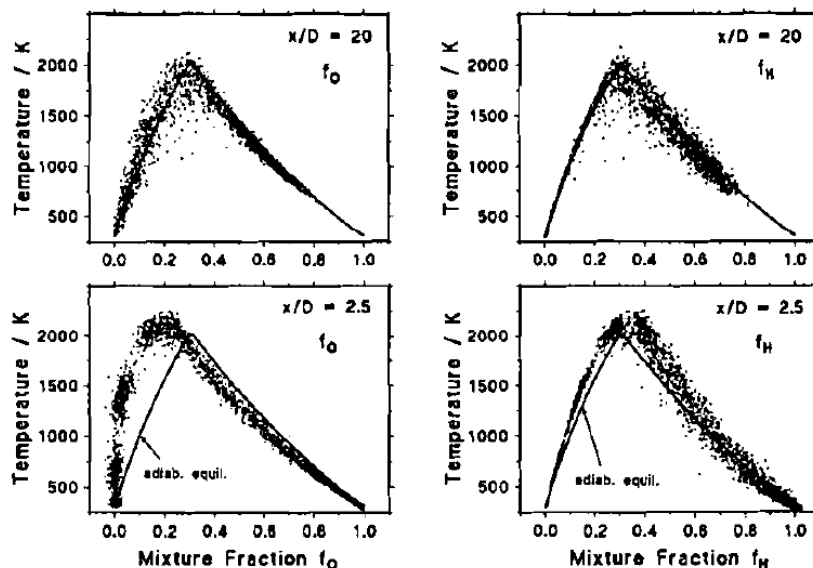


Figure 2.4: Temperature vs mixture fraction in comparison to adiabatic equilibrium. f_O is the mixture fraction based on element O and f_H is the mixture fraction based on element H. [25]

Another way to reduce computational time is to use a fast chemistry approach. Fast chemistry reduces the number of independent scalar variables. In this approach the equation for mixture fraction is solved instead of solving the transport equations for all separate species. The mixture fraction approach assumes that all species have equal diffusivities. The same diffusion coefficient is used for all species, which means that differential diffusion cannot be included in this approach as is. It is however possible to extend this model to include differential diffusion. First of all, the mixture fraction should be defined more precisely. Elements are not destroyed by chemical reactions, which means that element mass fractions are useful to use as a quantity to obtain a mixture fraction. Carbon, hydrogen and oxygen are usually used to obtain mass mixture fractions. Without differential diffusion, all element based mixture fractions, given by Equation 2.7, are identical. The advantage of describing the mixture fraction in this way is that it is easy to obtain a good approximation of mixture fraction from experimental data. Another way of expressing the mixture fraction was proposed by Bilger. Bilger's equation is shown in Equation 2.5 and 2.6 [10] where 1 is the oxidizer and 2 is the fuel stream. Bilger's mixture fraction requires that the stoichiometric value agrees with the value obtained using equal diffusivities. In the case of differential diffusion it is useful to compare values of different element based mixture fractions in experimental data to identify differential diffusion. Typically a scatter plot of values of two mixture fractions is made.

$$Z = \frac{Z_{un} - Z_{un,2}}{Z_{un,1} - Z_{un,2}} \quad (2.5)$$

$$Z_{un} = \frac{2Z_C}{M_C} + \frac{Z_H}{2M_H} - \frac{Z_O}{M_O} \quad (2.6)$$

Two problems that occur and can still be improved upon when including differential diffusion in fast chemistry are including differential diffusion in the flamelet calculation and in the turbulent equations. For the case of the flamelet equations, the problem is that a suitable mixture fraction needs to be defined in order to use detailed flamelets. Bilger's mixture fraction can be used to do this. In this way, the flamelet table can be organised with mixture fraction as the independent variable. Using this table will still not give accurate results as the simplification of $Le=1$ is still made in the laminar diffusion term. However, e.g. the flame temperature still has better predictions when using the table which includes differential diffusion effects. Including differential diffusion in the turbulent equations still needs to be investigated.

Including differential diffusion in specific combustion models will be explored in chapter 3.3.

2.2.2. Recreating the H3 Graphs

The graphs in Figure 2.4 have been recreated to check the data and get a better understanding of the flame. The results at $x/d=2.5$ are shown in Figure 2.5. The mixture fraction is calculated using a mixture fraction based on element mass fractions as shown in Equation 2.7 [45]. Here the subscript u refers to the unburnt state and subscript b refers to the burnt state.

$$Z = \frac{Z_i - Z_{i,b}}{Z_{i,u} - Z_{i,b}} \quad (2.7)$$

The adiabatic flame temperature is calculated using the fact that the unburnt and the burnt gases have the same specific enthalpy. Assuming constant pressure the flame temperature can be calculated using Equation 2.8 [45].

$$h_u = \sum_{i=1}^S Y_{i,u} h_{i,u} = \sum_{i=1}^S Y_{i,b} h_{i,b} = h_b \quad (2.8)$$

$$h_{i,b} = h_{i,u} + \int_{T_u}^{T_b} c_{p,i} dT$$

Figure 2.5 shows the results close to the nozzle ($x/d=2.5$). At the lean side the adiabatic flame temperature is again lower than the experimental temperature, showing that differential diffusion occurs. Hydrogen is a fast diffusing species which causes the effect to be stronger in the hydrogen curve compared to the oxygen curve. Meier states that the bulge in the oxygen curve corresponds to the radial position of the air side of the flame. Slow transport of H_2O and fuel- N_2 from the reaction zone to the air side can cause high concentrations of hot O_2 on the air side. When comparing the adiabatic curve of Figure 2.5 to Figure 2.4 it can be seen that they are not identical. This can be due to the fact that the curve in Figure 2.5 is calculated using major species only, while the other curve is calculated using all major and minor species.

2.2.3. Past Research

When looking at research in differential diffusion, some of the main combustion models that come up are CMC, transported PDF and flamelet models. An example of how CMC can be used (with a RANS simulation) is the work of Ma et al. [23]. Ma included differential diffusion in a CMC formulation for a non-premixed hydrogen-air flame. From the results it can be seen that the model gives a good prediction for some variables, but not for all. For example, differential diffusion effects can be seen at the position further from the nozzle, which is not expected. This can be due to the choice of the closure model. Ma suggests to use a LES model if one wishes to get better mean species predictions.

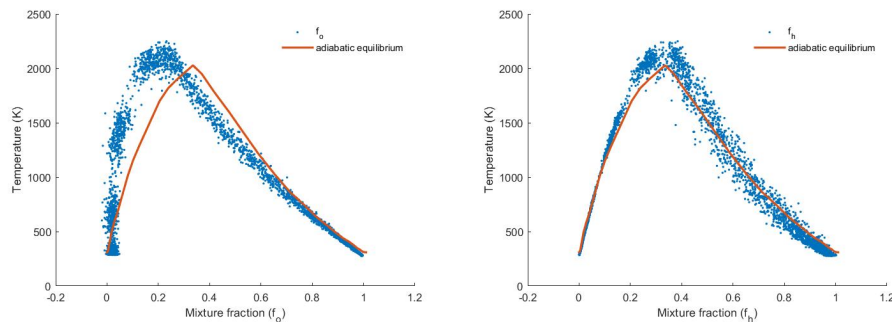


Figure 2.5: Temperature vs mixture fraction in comparison to adiabatic equilibrium at $x/d=2.5$. F_O is the mixture fraction based on element O and F_H is the mixture fraction based on element H.

There are several examples of using the PDF method to include differential diffusion but they are not explicitly for non-premixed turbulent diffusion flames. Richardson et al. [41] used a PDF mixing model to model premixed flames with differential diffusion. A new method was presented for accounting for differential diffusion in pairwise-exchange models by applying a correction term. The Interaction by Exchange with the Mean (IEM) and the Euclidian Minimum Spanning Tree (EMST) models are discussed. These models have been compared with DNS data in order to evaluate their performance. EMST gives the best results, but has a very large computational cost. If the flame structure is not critical IEM is the best choice. A different form of differential diffusion model is shown by Aksit et al. [1]. Soot particles have a very low diffusivity compared to gas phase species. Taking into account the diffusion of soot is also a form of differential diffusion. The simulation is done by coupling a conventional finite volume solver with a Monte Carlo simulation, and therefore creating a 'hybrid model'. Computational time is minimized by introducing all combustion chemistry (except for the soot formation) in a laminar flamelet approach. Soot is modelled in more detail with a two-step formulation. With this method, soot was still underpredicted but this was probably due to limitations of underlying scalar field predictions. The next paper that will be discussed is by Han et al. [19]. It focused on a turbulent lifted hydrogen flame and analysed among other things the flame sensitivity with respect to differential diffusion. A LES/PDF approach is used where differential diffusion is included in a Interaction-by-Exchange-with-the-Mean (IEM) model. When comparing cases with and without differential diffusion, some conclusions were drawn. Temperature, species mass fractions and lift-off height are very sensitive to differential diffusion, as H and H_2 do occur in the flame. Differential diffusion enhances auto-ignition near the base, but it also makes the flame more narrow in physical space. Zhou et al. [46] also used the LES method, but used a filtered density function (FDF) instead of a PDF based on a Monte Carlo particle solver. The flame used is a jet-in-hot-coflow methane-hydrogen flame. Five cases have been evaluated, with either differential diffusion in the mean drift term, in the subgrid term, both or neither. The case with differential diffusion in the drift term only gives the best results in the peak temperature and CO&OH fraction compared to the case without differential diffusion.

If one wants to use a flamelet model, there are several ways to do that. An example of a steady flamelet is the research by Wang [44]. He developed two modelling strategies to include differential diffusion in flamelet models. The turbulent non-premixed Sandia flame D was modelled using these models. The paper explains in detail how one can extend (steady) flamelet models to include differential diffusion. A linear and a non-linear differential diffusion model was made. When looking at piloted natural gas jet diffusion flames, it can be seen that the degree of differential diffusion can be predicted by power laws. When looking at the overall effect of differential diffusion in turbulence, the new models give more accurate results compared to an old differential diffusion model and an equal diffusivity model. Using a flamelet model in a RANS simulation while including differential diffusion is therefore deemed feasible.

Donini et al. [11] used the Flamelet Generated Manifold model (FGM) to research differential diffusion in Ansys-CFX. The flame used for the simulation is a stratified premixed cooled flame and therefore nothing like the H3 flame, but the article proves that the FGM is a viable option for modelling differential diffusion. Another flamelet model which modelled differential diffusion is by Pitsch et al. [33]. For this research, Fluent was used. Pitsch used an unsteady flamelet to model a steady turbulent $CH_4/H_2/N_2$ -air diffusion flame. The $k-\epsilon$ model is used with buoyancy and a correction for round jets. At first the unsteady flamelet model is

used with presumed PDF for mixture fraction (so differential diffusion is not taken into account). Different mechanisms that can cause differential diffusion to become important are discussed. The most important one is that the near field of jet diffusion flames might contain laminar structures. This would mean that turbulent mixing is not dominant and molecular diffusion should be taken into account. Another mechanism that Pitsch mentions to allow for differential diffusion in turbulent flows is that the value of the molecular diffusivity of a species is in the same order of magnitude as the turbulent diffusivity. Finally it is stated that a laminar layer can exist in the mixing layer which is governed by differential diffusion. Pitsch concludes that the unsteady flamelet model can describe most of the flame correctly. Close to the nozzle a previously developed flamelet formulation capable of describing differential diffusion can be used.

From the research on differential diffusion it becomes clear that there are many ways to try and include differential diffusion into already existing models. A LES or even DNS model would give the best (most detailed) results, but given the timeframe for a thesis, it is best to start in a RANS frame and only use LES if time permits. The flamelet models, flamelet generated manifold in particular, seem the most promising when one wants to work with Ansys Fluent, but transported PDF is also a good candidate.

3

Computational Models

In this chapter the proposed models are introduced and elaborated. Finally a model choice is made and the method will be elaborated.

When computing a turbulent diffusion model, three different submodels can be recognized: turbulent model, chemical model and a coupling model which couples the first and second model. Figure 3.1 shows an overview of turbulent combustion models which are included in Ansys Fluent. With the limited resources available, it is good to choose a model that has a low computational time. The research will use a RANS approach. An overview of all the governing equations used in a RANS approach can be found in Turbulent Combustion Modelling [14] or Theoretical and Numerical Combustion [35]. In this study Ansys Fluent software will be used, since it offers a quite broad range of modelling approaches for turbulent non-premixed flames. Section 3.4 will define the models chosen for this study.

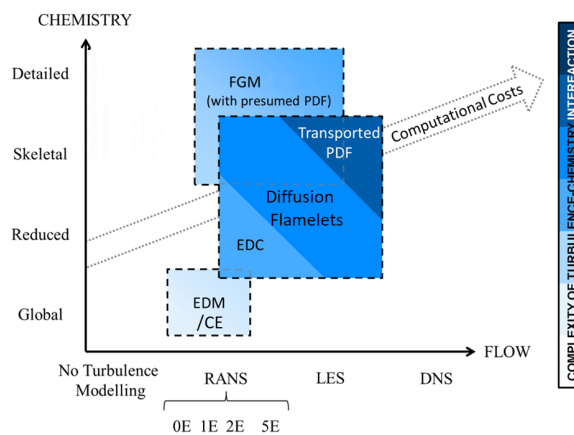


Figure 3.1: Schematic overview of modelling approaches for turbulent combustion (adapted from Perpignan et al. [31])

3.1. Chemical Model

In order to describe the chemical processes a chemical model is needed. When all species and reactions are taken into account this can lead to quite an extensive calculation. To reduce the computational time, reduced chemistry schemes are very effective. They only take a small number of species and reactions into account. A disadvantage of this is that such systems are usually only accurate for a range of conditions.

Two schemes that have been considered were by Li et al. [22] and by Burke et al. [5]. The mechanism from Li et al. has been used to model the H3 flame before. The mechanism by Burke et al. was based on the mechanism by Li et al. but had improvements on the rate constant and transport treatment. These improvements mostly

had an effect on high pressure cases and therefore it was chosen to use the mechanism by Li et al. as the H3 flame is a flame at atmospheric pressure.

The mechanism described by Li et al. is a chemical reaction mechanism for H_2/O_2 . The mechanism contains 19 different reversible reactions for 9 different species (H_2 , N_2 , O_2 , H_2O , H , O , OH , HO_2 and H_2O_2), where the user can choose to use either Ar, He or N_2 as system dilutant.

3.2. Turbulence Model

There are several different RANS turbulence models in Fluent, e.g. the $k-\varepsilon$ model, $k-\omega$ model and the Reynold Stress Model (RSM). The $k-\varepsilon$ model is the most popular one and is also used in a lot of the past H3 research. The $k-\varepsilon$ and $k-\omega$ models are quite similar, the biggest difference is that $k-\omega$ performs better near a wall while $k-\varepsilon$ gives better predictions far from a boundary. Since H3 is an open flame, $k-\omega$ will not be considered. Information on the models in the next sections is obtained from Ansys [2],[3], Poinso et al. [35] and Agryropoulos et al. [4].

3.2.1. $k-\varepsilon$ Model

The $k-\varepsilon$ model is a 2-equation model which is widely used despite its limitations. It is a robust model but it is unable to work with severe pressure gradients and extra strains. The model is suitable for initial iterations, rough estimations and parametric studies. The turbulent viscosity is described by formula 3.1 [35]. Here C_μ is a model constant while k (turbulent kinetic energy) and ε (turbulent dissipation rate) are the two unknowns that need to be solved using the two equations given in 3.2 and 3.3 [35]. Here σ_k , σ_ε , $C_{\varepsilon 1}$ and $C_{\varepsilon 2}$ are model constants. Their usual values of all constants are shown in Table 3.1 [35]. P_k is the source term which can be seen in Equation 3.4 [35].

$$\mu_T = \bar{\rho} C_\mu \frac{k^2}{\varepsilon} \quad (3.1)$$

$$\frac{\partial}{\partial t}(\bar{\rho}k) + \frac{\partial}{\partial x_i}(\bar{\rho}\tilde{u}_i k) = \frac{\partial}{\partial x_i} \left[\left(\mu + \frac{\mu_t}{\sigma_k} \right) \frac{\partial k}{\partial x_i} \right] + P_k - \bar{\rho}\varepsilon \quad (3.2)$$

$$\frac{\partial}{\partial t}(\bar{\rho}\varepsilon) + \frac{\partial}{\partial x_i}(\bar{\rho}\tilde{u}_i \varepsilon) = \frac{\partial}{\partial x_i} \left[\left(\mu + \frac{\mu_t}{\sigma_\varepsilon} \right) \frac{\partial \varepsilon}{\partial x_i} \right] + C_{\varepsilon 1} \frac{\varepsilon}{k} P_k - C_{\varepsilon 2} \bar{\rho} \frac{\varepsilon^2}{k} \quad (3.3)$$

$$P_k = -\bar{\rho} \overline{u_i'' u_j''} \frac{\partial \tilde{u}_i}{\partial x_j} \quad (3.4)$$

C_μ	σ_k	σ_ε	$C_{\varepsilon 1}$	$C_{\varepsilon 2}$
0.09	1.0	1.3	1.44	1.92

Table 3.1: Values of emperical constants in $k-\varepsilon$ model as proposed by Poinso et al. [35]

There are many variations on the $k-\varepsilon$ model of which the realizable $k-\varepsilon$ model and the renormalization group $k-\varepsilon$ model are the most important ones. The realizable model is more suited for jets and mixing layers, channels, boundary layers and separated flows. An important difference with the standard model is that the constant C_μ is not a constant anymore but is computed by an eddy-viscosity equation. In the study of jet flames, the $k-\varepsilon$ models are often used with a modified value of the model constraints in order to have a better prediction of the velocity field before focusing on turbulence-chemistry interaction. The formulas for the realizable model as used in Ansys can be found in Equation 3.5, 3.6 and 3.7 [3]. G_k represents the generation of turbulent kinetic energy due to velocity gradients, G_b is the generation of kinetic energy due to buoyancy and Y_M is the contribution of fluctuating dilatation in compressible turbulence to the overall dissipation rate. A_0 , A_s , C_1 , C_2 , $C_{1\varepsilon}$ and $C_{3\varepsilon}$ are model constants, while S_k and S_ε are used defined source terms.

$$\frac{\partial}{\partial t}(\rho k) + \frac{\partial}{\partial x_j}(\rho k u_j) = \frac{\partial}{\partial x_j} \left[\left(\mu + \frac{\mu_t}{\sigma_k} \right) \frac{\partial k}{\partial x_j} \right] + G_k + G_b - \rho\varepsilon - Y_M + S_k \quad (3.5)$$

$$\frac{\partial}{\partial t}(\rho\varepsilon) + \frac{\partial}{\partial x_j}(\rho\varepsilon u_j) = \frac{\partial}{\partial x_j} \left[\left(\mu + \frac{\mu_t}{\sigma_\varepsilon} \right) \frac{\partial \varepsilon}{\partial x_j} \right] + \rho C_1 S\varepsilon - \rho C_2 \frac{\varepsilon^2}{k + \sqrt{v\varepsilon}} + C_{1\varepsilon} \frac{\varepsilon}{k} C_{3\varepsilon} G_b + S_\varepsilon \quad (3.6)$$

$$C_\mu = \frac{1}{A_0 + A_s \frac{kU_*}{\varepsilon}} \quad (3.7)$$

3.2.2. Reynold Stress Model

The RSM is more complete compared to the $k - \varepsilon$ model. It is most suitable for complex 3D flows with strong swirl/rotation. The RSM avoids using the eddy viscosity assumption to close the equations. Closure of the model is done by solving the Reynolds Stress tensor directly via 7 transport equations (in 3D). Usually RSM is more complex and requires more CPU time compared to the $k - \varepsilon$ model. Therefore it is primarily used in flows where the $k - \varepsilon$ model cannot accurately model the flow.

3.3. Combustion Model

Combustion models or turbulence-chemistry models are used to model the interaction between the turbulence model and the chemistry model. When looking at non-premixed combustion, Fluent offers the following models: Eddy Dissipation model, Eddy Dissipation Concept (EDC), Chemical Equilibrium (CE), Steady and Unsteady Diffusion Flamelet, Flamelet Generated Manifold (FGM) and Composition PDF Transport (T-PDF). The chemical equilibrium model is not detailed enough to include differential diffusion. The EDC can include differential diffusion, but only in the laminar flux. All the flamelet models can include diffusion, but the FGM has the advantage of including many species and differential diffusion in the flamelets. T-PDF has many advantages and can be extended to include a micromixing model for differential diffusion, but is relatively difficult to use compared to the flamelet models and is costly. Table 3.2 gives a summary of the models mentioned and their abilities. The transported-PDF and FGM seem to be the models that will give the best results in a RANS model in Fluent. It can also be seen from past research in section 2.2 that FGM and transported PDF models are most likely the best choice for studying the H3 flame when one wants to include the effects of differential diffusion.

	Detailed Chemistry	Differential diffusion	Turbulent fluctuations included
Chemical Equilibrium	No	No	Yes in PDF (Z)
Eddy dissipation model	One step model	In mean equations	No
Eddy Dissipation Concept	Yes	In mean equations	No
Flamelet Generated Manifold	Yes	Yes, in flamelets	Yes, in PDF (Z,c)
Transported-PDF	Yes (costly)	Extension needed	Yes, fully

Table 3.2: Non-premixed combustion models included in Ansys Fluent and their properties

3.3.1. Transported PDF Model

All information for the transported PDF method has been obtained from Ansys [3], Warnatz et al. [45] and the lectures of the AE4262 course at the TU Delft.

The transported PDF method is a good way to model non-premixed turbulent diffusion flames. When using RANS, the particle Monte-Carlo method (also known as Lagrangian method in Ansys) is the most suitable. The idea of the transported PDF is to extend the Reynolds-averaging by deriving a transport equation for their single-point, joint PDF. This PDF represents the fraction of time that the mixture spends in a certain state. The PDF transport equation is derived from the Navier-Stokes equations and can be seen in formula 3.8 [3]. Here P is the PDF, ρ is the Reynolds-averaged density, u_i is the Favre mean velocity vector while u''_i is the velocity fluctuation vector, S_k is the reaction rate, ψ is the composition space vector and $J_{i,k}$ is the molecular diffusion flux vector. Note that the left hand side is closed.

$$\frac{\partial}{\partial t}(\rho P) + \frac{\partial}{\partial x_i}(\rho u_i P) + \frac{\partial}{\partial \psi_k}(\rho S_k P) = -\frac{\partial}{\partial x_i}[\rho \langle u_i'' | \psi \rangle P] + \frac{\partial}{\partial \psi_k} \left[\rho \left\langle \frac{1}{\rho} \frac{\partial J_{i,k}}{\partial x_i} | \psi \right\rangle P \right] \quad (3.8)$$

The PDF depends on many independent variables. This causes high computational cost. In order to minimize this, the Monte-Carlo method was introduced. The PDF is represented by stochastic particles. These particles mimic the evolution of the PDF. The joint PDF is reduced to a PDF for scalars to treat the chemical reaction and the velocity field is computed by the turbulence model. They are coupled using the density. A new flow field is calculated and this is used in the PDF. The transported PDF uses a lot of computational time. It is therefore advised to use it in 2D models. In order to reduce the computational time it is also advised to use a reduced chemistry scheme.

Ansys has three different models for the molecular diffusion in the Lagrangian model: Modified Curl model, Interaction by Exchange with the Mean (IEM) model and Euclidean Minimum Spanning Tree (EMST) model. The Modified Curl model randomly chooses pairs of particles and their compositions are moved toward the mean composition. The IEM model moves the composition of all the particles towards the mean. The EMST model mixes particles that are next to each other in composition space. Particles that are close in composition space are mixing with each other. The EMST model is usually more accurate due to its localness in composition space, but has a greater computational expense. IEM has the lowest accuracy. It is not yet clear which of these models works best when one wants to include differential diffusion. Ansys Fluent does have a micromixing option which can offer opportunities. The essential problem is that the models provided are mostly based on composition whereas differential diffusion is based on gradients. Ansys-Fluent does not include the option to include differential diffusion, but it can be added with the help of user-defined functions. Transported-PDF therefore seems promising to use in this thesis.

3.3.2. Flamelet Generated Manifold Model

All information on the flamelet generated manifold has been obtained from Ansys [3], van Oijen et al. [43] and the lectures of the AE4262 course at the TU Delft.

The Flamelet Generated Manifold (FGM) assumes a fixed flame structure. Models for the basic premixed flamelet model and non-premixed laminar flamelet model are combined in order to get the FGM model. It assumes that the scalar evolution in a turbulent flame can be approximated by the scalar evolution in a laminar flame. In principle the FGM model works as follows. First, a collection of flamelets is either computed by Ansys or imported from another source. These flamelets should be representative of the combustion system, so in this case of a non-premixed flame. A progress variable needs to be defined. The flamelets are usually expressed as a function of the mixture fraction Z and the (normalized) reaction progress variable c . In the case of a turbulent flame the influence of statistical fluctuations is also included. The created lookup table is then coupled with a CFD code. The transport equations are solved using the variables found in the lookup table. As burning steady flames do not reveal information on states with low values of progress variables, extinguishing flames have been added to the flamelet library to cover the lower values. The formula for the progress variable can be seen in Equation 3.9. Here Y_k is the species mass fraction of k , where subscript eq is chemical equilibrium at the flame outlet and subscript u is the unburnt reactant at the flame inlet. α_k is a constant which in Ansys is zero by default and 1 for α_{H_2O} in the case of hydrogen combustion. The 1D adiabatic flamelet equations for partially premixed flames as presented in Ansys can be seen in Equation 3.10 and 3.11. It is specifically mentioned that these equations neglect differential diffusion.

$$c = \frac{\sum_k \alpha_k (Y_k - Y_k^u)}{\sum_k \alpha_k (Y_k^{eq} - Y_k^u)} \quad (3.9)$$

$$\rho \frac{\partial Y_k}{\partial t} + \frac{\partial Y_k}{\partial c} \dot{\omega}_c = \rho \chi_c \frac{\partial^2 Y_k}{\partial c^2} + \dot{\omega}_k \quad (3.10)$$

$$\rho \frac{\partial T}{\partial t} + \frac{\partial T}{\partial c} \dot{\omega}_c = \rho \chi_c \frac{\partial^2 T}{\partial c^2} - \frac{1}{c_p} \sum_k h_k \dot{\omega}_k + \frac{\rho \chi_c}{c_p} \left(\frac{\partial c_p}{\partial c} + \sum_k c_{p,k} \frac{\partial Y_k}{\partial c} \right) \frac{\partial T}{\partial c} \quad (3.11)$$

As stated before, in the case of a turbulent flame, the influence of statistical fluctuations is also included. This is done by creating an integrated PDF table that is characterised by the means and variances of the progress

variable and the mixture fraction. The transport equations of the variables used to characterise this PDF are shown in Equation 3.12, 3.13, 3.14 and 3.15.

Equation for mean mixture fraction:

$$\frac{\partial}{\partial t} \bar{\rho} \bar{Z} + \frac{\partial}{\partial x_i} (\bar{\rho} \bar{v}_i \bar{Z}) = \frac{\partial}{\partial x_i} \left(\bar{\rho} \bar{D}_{eff} \frac{\partial}{\partial x_i} \bar{Z} \right) \quad (3.12)$$

Equation for variance of mixture fraction:

$$\frac{\partial}{\partial t} \bar{\rho} \overline{Z'^2} + \frac{\partial}{\partial x_i} (\bar{\rho} \bar{v}_i \overline{Z'^2}) = \frac{\partial}{\partial x_i} \left(\bar{\rho} \bar{D}_{eff} \frac{\partial}{\partial x_i} \overline{Z'^2} \right) + 2\bar{\rho} \bar{D}_{eff} \frac{\partial \bar{Z}}{\partial x_i} \frac{\partial \bar{Z}}{\partial x_i} - C_\phi \bar{\rho} \frac{\varepsilon}{k} \overline{Z'^2} \quad (3.13)$$

Equation for mean unscaled progress variable:

$$\frac{\partial}{\partial t} \bar{\rho} \bar{Y}_c + \frac{\partial}{\partial x_i} (\bar{\rho} \bar{v}_i \bar{Y}_c) = \frac{\partial}{\partial x_i} \left(\bar{\rho} \bar{D}_{eff,c} \frac{\partial}{\partial x_i} \bar{Y}_c \right) + \bar{\rho} \bar{S}_k \quad (3.14)$$

Equation for variance of unscaled progress variable:

$$\frac{\partial}{\partial t} \bar{\rho} \overline{Y_c'^2} + \frac{\partial}{\partial x_i} (\bar{\rho} \bar{v}_i \overline{Y_c'^2}) = \frac{\partial}{\partial x_i} \left(\bar{\rho} \bar{D}_{eff,c} \frac{\partial}{\partial x_i} \overline{Y_c'^2} \right) + 2\bar{\rho} \bar{D}_{eff,c} \frac{\partial \bar{Y}_c}{\partial x_i} \frac{\partial \bar{Y}_c}{\partial x_i} - C_\phi \bar{\rho} \frac{\varepsilon}{k} \overline{Y_c'^2} + \bar{\rho} (\overline{S_c Y_c} - \overline{S_k Y_c}) \quad (3.15)$$

Differential diffusion can be included in several ways. Donini et al. [11] used a version of the FGM equations to include differential diffusion. In a previous research [8] transport equations were derived for c , h and Z . These formulas were adapted and the new formulas are shown in equations 3.16, 3.17 and 3.18 [11]. The first term on the right hand is the differential diffusion term. The case studied by Donini is a laminar premixed flame, which is different from the turbulent non-premixed flame used in this research. However, these formulas can give an idea of how the FGM can be adapted to include differential diffusion. Another way to include differential diffusion is to import PDF integrated tables from an FGM which are created using CHEM1D including differential diffusion. Research done by Ramaekers et al. [37] shows that it is indeed possible to use a CHEM1D data in Ansys Fluent. This option seems to be the most promising for including differential diffusion in Fluent.

$$\frac{\partial(\rho c)}{\partial t} + \nabla \cdot (\rho v c) - \nabla \cdot \left(\frac{\lambda}{c_p} \nabla c \right) = \nabla \cdot \left(\frac{\lambda}{c_p} \sum_{i=1}^{N_s} \alpha_i \left(\frac{1}{Le_i} - 1 \right) \nabla c \right) + \dot{\omega}_y \quad (3.16)$$

$$\frac{\partial(\rho h)}{\partial t} + \nabla \cdot (\rho v h) - \nabla \cdot \left(\frac{\lambda}{c_p} \nabla h \right) = \nabla \cdot \left(\frac{\lambda}{c_p} \sum_{i=1}^{N_s} h_i \left(\frac{1}{Le_i} - 1 \right) \nabla Y_i \right) \quad (3.17)$$

$$\frac{\partial(\rho Z)}{\partial t} + \nabla \cdot (\rho v Z) - \nabla \cdot \left(\frac{\lambda}{c_p} \nabla Z \right) = \nabla \cdot \left(\frac{\lambda}{c_p} \sum_{i=1}^{N_s} \zeta_i \left(\frac{1}{Le_i} - 1 \right) \nabla Y_i \right) \quad (3.18)$$

3.4. Model Choices

The goal of this thesis is to include differential diffusion in a RANS model of the H3 flame in Ansys Fluent. In order to do this, a model has to be build. Using the information from the previous sections, some decisions were made regarding the models used. As a chemical model the model described by Li et al. will be used. This model is a simplified description of hydrogen combustion but is still accurate enough to describe the major reactions and species. The $k - \varepsilon$ model will be used as turbulent model because of its robustness and previous success in other research. The combustion model will need changes in order to include differential diffusion. The most promising models seem to be FGM and T-PDF. In the case of FGM, differential diffusion can be included in flamelets produced by CHEM1D which can be imported in Ansys either as FGM or as a user defined PDF table using existing methods. T-PDF however will need new user defined functions in order to include differential diffusion and has a higher computational cost. It is therefore chosen to use the FGM model in this work. The final model will be build in several steps to get the final result. First, a model will be made using chemical equilibrium in order to make sure that the basics of the model are correct and the results roughly match the experimental data. The second step is to use the steady diffusion flamelet model to refine these results and start incorporating flamelets. Finally the FGM model will be used where differential diffusion will be included in the flamelets using CHEM1D. This final model will be validated using the data obtained by Meier [25] and Pfuderer [32].

3.4.1. UDF with CHEM1D

As stated in the previous section it is possible to include differential diffusion in the FGM model and use this in Fluent. An explanation of the proposed method will be given here. The information in this section has been obtained from files provided by Likun Ma, Mengmeng Ren and Naiara Romero-Anton.

The CHEM1D tool from TU Eindhoven is used, which uses one dimensional flame code to construct flamelets. The first step is to calculate counterflow flames using CHEM1D, in this case the non-premixed hydrogen-nitrogen flame is used as input. Several inputs can be adjusted in a defaults.csf file such as the flame type, simulation type, boundary conditions, fuel- and oxidizer composition, reaction mechanism and desired strain rate. In order to get a complete range of flamelets covering the entire flame, both steady and unsteady (stationary and time dependent) calculations are made. In the case of an adiabatic flame, the strain rates will be varied to get these different flamelets. First steady calculations of different strain rates are done until the flame extinguishes, after this unsteady calculations are run at the extinction strain rate with the last stable flame as the start solution file.

The steady and unsteady flamelets that have been created can now be combined to an FGM table using Matlab code. This code calculates the progress variable (which in the case of the H3 flame is water) at each grid point of each flamelet. The data for states with low value of progress variable are provided by the extinguishing flamelets. Several other properties such as density and specific heat can either be calculated using the thermoprop tool or can be read directly from CHEM1D. All flamelets are stored in a matrix with 3 dimensions where the first is the progress variable, the second is the mixture fraction and the third represents all of the output variables. This matrix is written into a text file, but this file cannot be read by Fluent. There are two options to continue: either change the file format to the FGM format that Fluent uses, or create a PDF integrated table and import this in Fluent using a user defined function (UDF).

In order to use the UDF, the FGM table needs to be integrated to a PDF table containing the mean properties as a function of mean and variance of mixture fraction and progress variable. The probability is calculated according to the β -function. This is also done using Matlab code. As the new PDF table does not have the same format as the PDF tables from Fluent, it is hard to import it on its own. The UDF solves this issue as it overwrites the PDF table from Fluent with values from the new PDF table. In order to use the table properly one should also overwrite the definition of the progress variable in Fluent to the definition of the progress variable as used in the FGM.

4

Results and Discussion

This chapter contains the results from this work. The CHEM1D flamelets are discussed, results from Fluent are presented and analysed and these results are compared both to each other and to other research.

4.1. CHEM1D

CHEM1D is a tool developed by TU Eindhoven which can generate both steady and unsteady flamelets. These flamelets can be coupled using Matlab code and can be used as a flamelet generated manifold input for e.g. Ansys Fluent or OpenFOAM. This section will talk about the settings used in CHEM1D and compare the flamelets generated by CHEM1D to the experimental data.

4.1.1. Setup of CHEM1D

Following the method explained in Section 3.4.1 a set of flamelets was calculated and combined to an FGM. The Lewis model was used for transport to ensure that the calculations were done using the different Lewis number of all the species. This is necessary to include the effect of differential diffusion. In the case of the H3 flame in combination with the Lewis model the last strain rate was 9110 s^{-1} . The fuel and oxidiser were the same as for the H3 flame, a mixture of hydrogen diluted with nitrogen on 50/50 volume ratio and air as oxidizer. The Li mechanism is used to describe the chemical reactions.

4.1.2. Results of CHEM1D compared to Data

The results of CHEM1D are compared to the available data to see if the created flamelets are of sufficient value. The progress of the combustion process can be described using a progress variable. In the case of hydrogen combustion the immediate choice for a progress variable is the mass fraction of the water vapour, so that $Y_c = Y_{H_2O}$ [28]. Water can describe the advancement of reaction after ignition. Figure 4.1 shows the temperature vs. the progress variable. The color scale represents the mixture fraction where a mixture fraction of 1 means fuel and a mixture fraction of 0 means air. The top branch is therefore the lean branch, while the bottom branch is the rich branch. The main flamezone is around $Z=0.2-0.4$. When comparing these graphs it can be seen that they are in good agreement when it comes to the shape. The mixture fraction pattern does differ a bit but is overall still in good agreement.

Another set of graphs that is interesting to compare is the mixture fraction with the mixture fraction of specific species, in this case of hydrogen and oxygen. These can be seen in Figures 4.2 and 4.3. Here the color represents the progress variable. It can be seen that the progress variable is overall in agreement but the shape of the data is a large cloud whereas CHEM1D is represented by a narrow line. This difference can be explained by experimental error and presence of a wider variety of flame type, while CHEM1D purely describes a specific flame type. These graphs can show if differential diffusion is present. In the absence of differential diffusion $Z_O = Z_H = Z_{BLGR}$ (Bilger's mixture fraction) which would result in a straight line. Any deviations from this straight line therefore indicate the presence of differential diffusion. Differential diffusion is shown more clearly in the CHEM1D graphs than the data, and in the CHEM1D graphs hydrogen shows a larger deviation

than oxygen. The latter is due to the fact that oxygen contributes more to the Bilger mixture fraction than hydrogen. Differential diffusion of hydrogen can have an effect on the combustion, as hydrogen is leaking away from the fuel compared to the nitrogen, which leads to a quick drop of hydrogen at the fuel side.

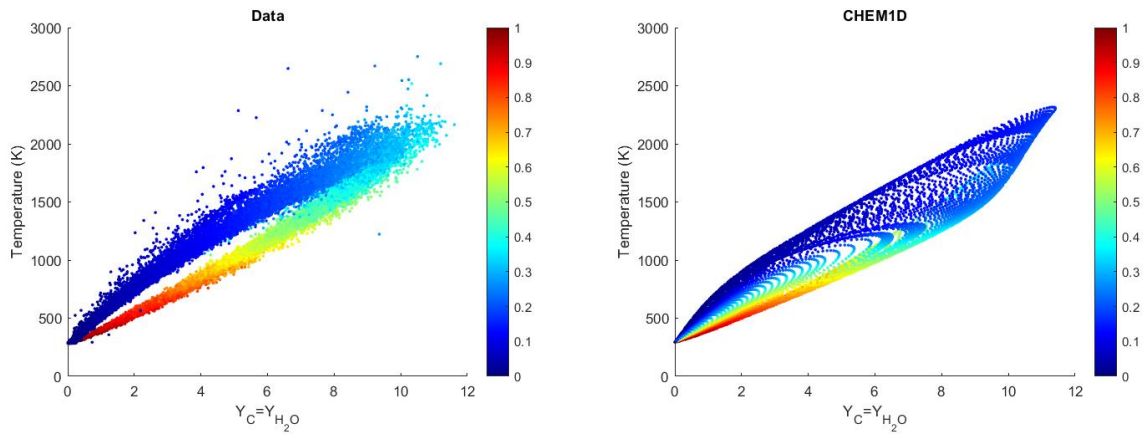


Figure 4.1: Temperature vs Progress variable for the data (left) and CHEM1D (right), where the color represents the mixture fraction

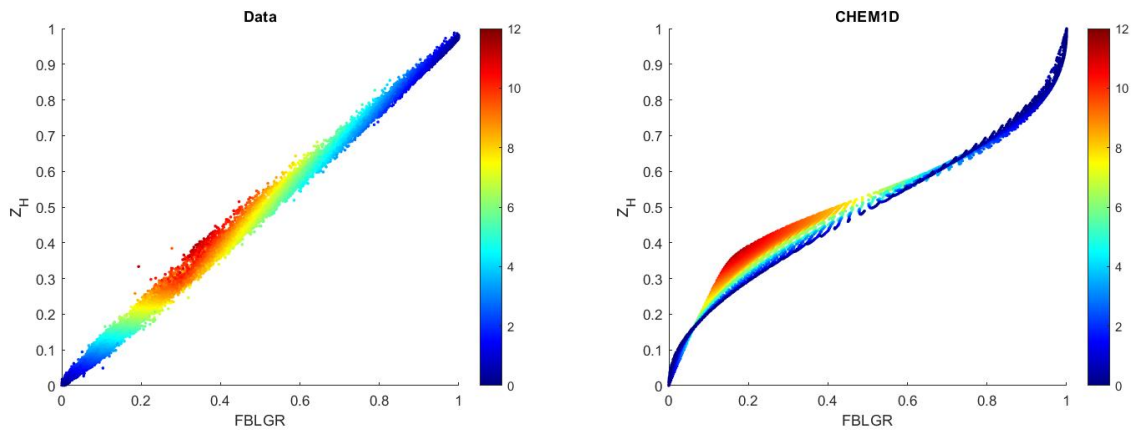


Figure 4.2: Mass fraction of hydrogen element vs mixture fraction for the data (left) and CHEM1D (right), where the color represents the progress variable

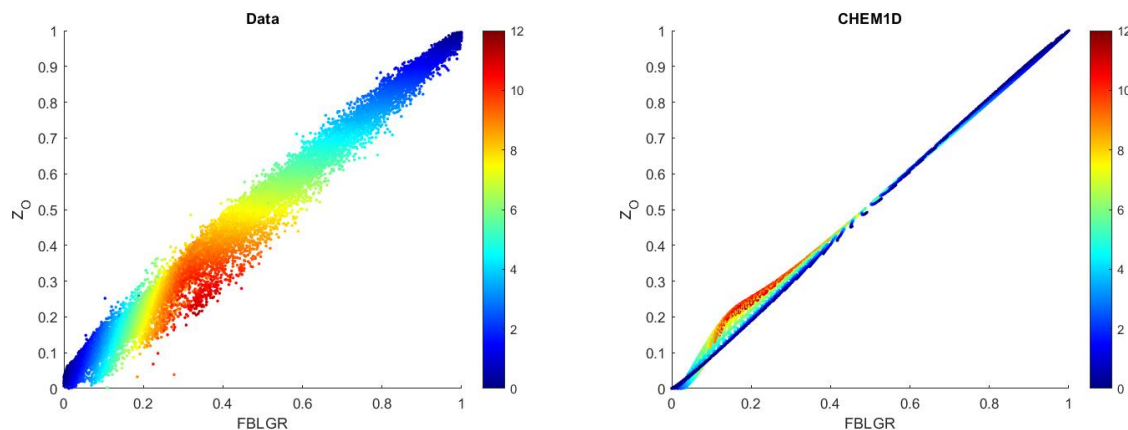


Figure 4.3: Mass fraction of oxygen element vs mixture fraction for the data (left) and CHEM1D (right), where the color represents the progress variable

In Figure 4.4 the mixture fraction vs progress variable graphs can be seen. The CHEM1D flamelets consist of steady and unsteady flamelets which together should describe every stage of the flame. The data only represent the burning flamelets, apart from a few cases with a low progress variable. When comparing the data to the CHEM1D flamelets it can be seen that both the shape and magnitude of the flamelets are in agreement, but the position of the peak is at stoichiometric ratio (0.31) in the data while it shifted to 0.2 in CHEM1D. This is due to the fact that differential diffusion is incorporated. In Figure 4.5 two different CHEM1D results are shown, the only difference between the two is that for one the Lewis numbers are equal to unity while for the other one the Lewis numbers are equal to their actual values. Using unity Lewis numbers results in flamelets with the peak at the right mixture fraction, but the progress variable values are lower overall. Changing the Lewis numbers to the actual values gives the right overall maximum of progress variable. A mismatch can be seen between the experiments and the flamelet data on the rich side, which can cause underpredictions in rich mixtures, often close to the nozzle. Section 4.5 will discuss which of the two flamelets will give the best results.

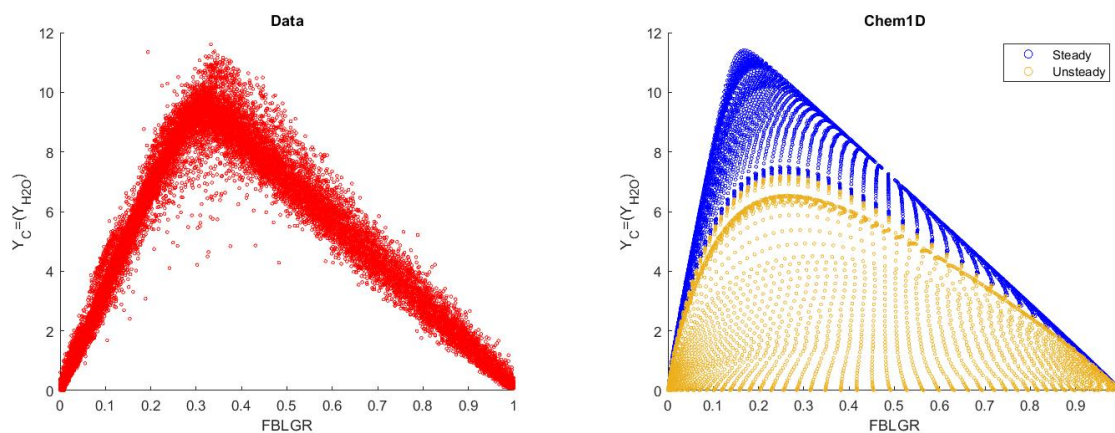


Figure 4.4: Progress variable vs mixture fraction for the data (left) and CHEM1D (right)

Finally, in Figure 4.6 the relation between temperature and the mixture fraction based on hydrogen and oxygen are compared to the data. Figure 2.4 from Meier et al. already showed that for both Z_O and Z_H differential diffusion is present. The flamelets do account for the differential diffusion, but do not agree with the data very well. Since the effect of differential diffusion is the one that is supposed to be included in the calculations, it was decided to use these flamelets even though there are some differences between the data and the CHEM1D flamelets. A CHEM1D simulation without differential diffusion will however also be included for a comparison.

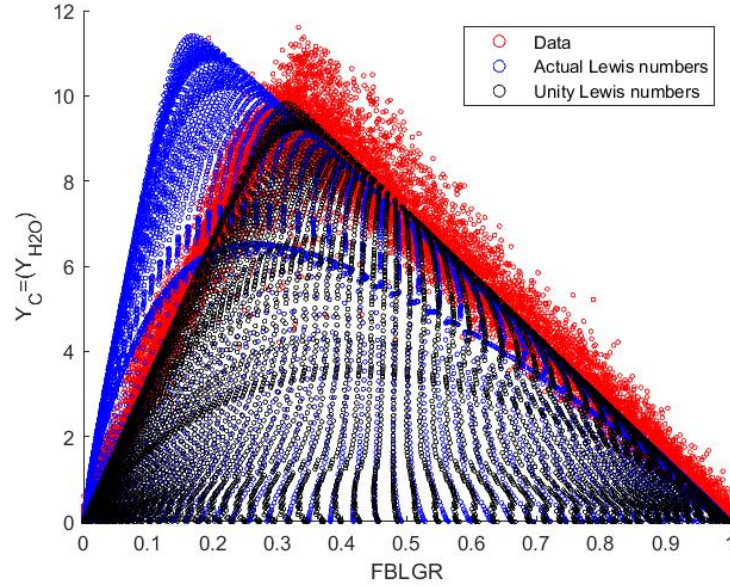


Figure 4.5: Progress variable vs mixture fraction for CHEM1D with and without unity Lewis numbers and the Data

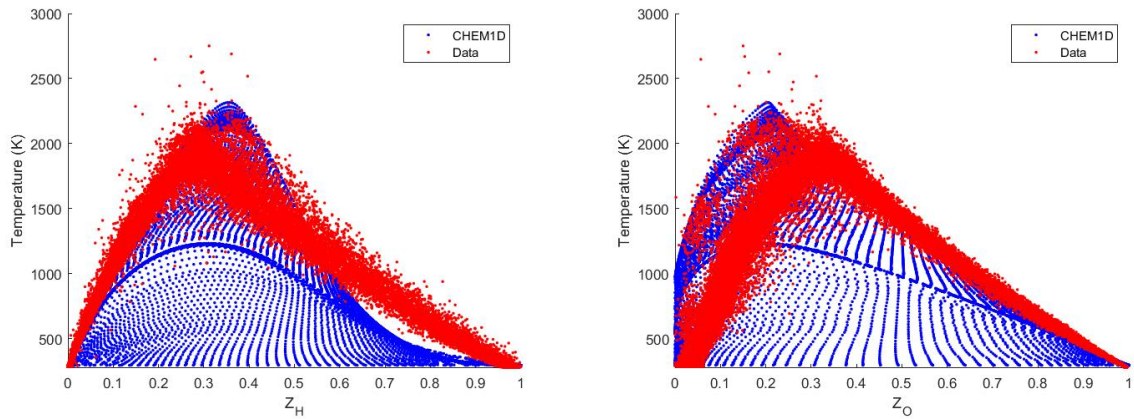


Figure 4.6: Temperature vs mixture fraction based on hydrogen element (left) and oxygen element (right)

4.2. Turbulent Flame Simulation

This section is about the H3 flame properties, the geometry and mesh used and the conditions used in Ansys Fluent in order to model this flame.

4.2.1. Case Description

The flame that is simulated is the H3 flame [25]. It is a jet diffusion flame with a hydrogen and nitrogen fuel. The ratio of hydrogen to nitrogen is 50/50 with a stoichiometric ratio of 0.31. The fuel enters from a nozzle with a diameter of 8 mm and a speed of 34.8 m/s. A co-flow of air surrounds the fuel in a contoured nozzle with a diameter of 140 mm and a speed of 0.2 m/s. A sketch of the setup can also be seen in Figure 4.7.

4.2.2. Mesh Setup

For the modelling of the H3 flame the CFD program Ansys Fluent 18.2 is used. The reason that not the most recent version of Ansys Fluent was used is that it was more compatible with the UDF which will be used later on. To see if differential diffusion can be included in the model, a 2D, axisymmetric RANS model should

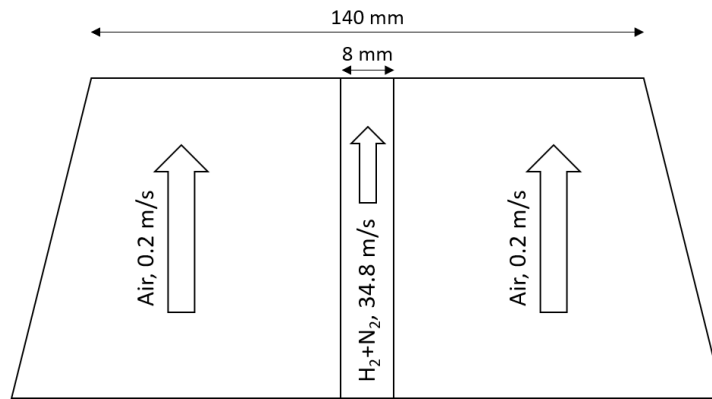
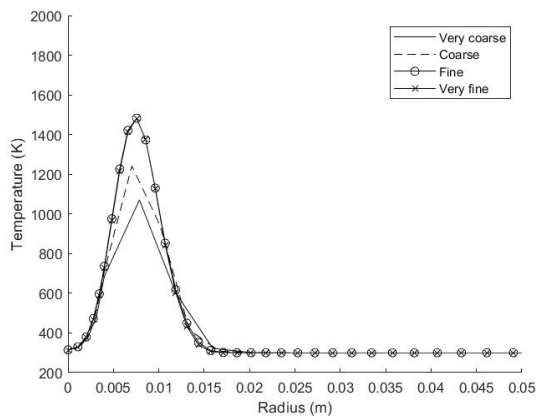
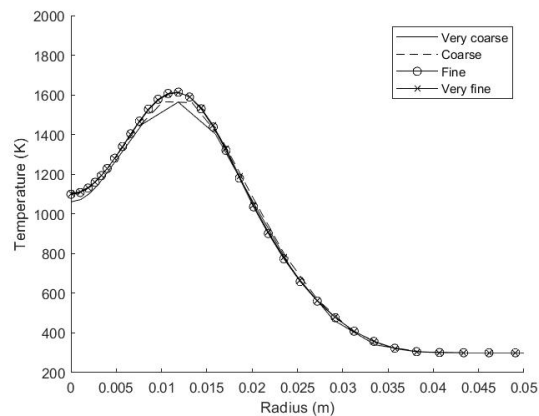


Figure 4.7: Setup of the H3 flame

suffice. Since axisymmetry is used, a domain with extension in axial and radial direction is used. The mesh is created using the meshing program provided by Ansys. The simulation domain has a radius of $37.5 d$ and a length of $125 d$. In addition a part of the fuel pipe is included. This domain is large compared to previous research. For example, D'Ausilio [13] had a domain of $18.75 d$ by $81.25 d$. In this case however a smaller domain led to backflow problems at the domain boundary that kept the model from converging, which is why a larger domain was used. In order to find a mesh with a good convergence, several different mesh layouts were tested. Since the shape of the domain consists of 2 rectangles, the choice was made to use rectangular elements in the mesh. Mesh stretching was used to increase the size of the elements, which started at the flame base. This can also be seen in Figure 4.10. The very coarse mesh has 6,208 cells, the coarse mesh has 10,037 cells, the fine mesh has 15,856 cells (Figure 4.11, left) and the very fine mesh has 31,312 cells (Figure 4.11, right). From the graphs in Figures 4.8 and 4.9 it can be seen that the two coarse meshes result in a temperature profile that is not fully converged, while the two fine meshes agree on the temperature profile. The computational time for the fine and very fine mesh does not differ noticeably, so the very fine mesh would be preferred. However, for some cases the very fine mesh (and even finer meshes) did cause a numerical oscillation in the flame which can be solved by changing the solution controls. This should be taken into account when performing calculations.

Figure 4.8: Temperature profiles for different meshes at $x/D=2.5$, using the chemical equilibrium model with the Li mechanismFigure 4.9: Temperature profiles for different meshes at $x/D=20$, using the chemical equilibrium model with the Li mechanism

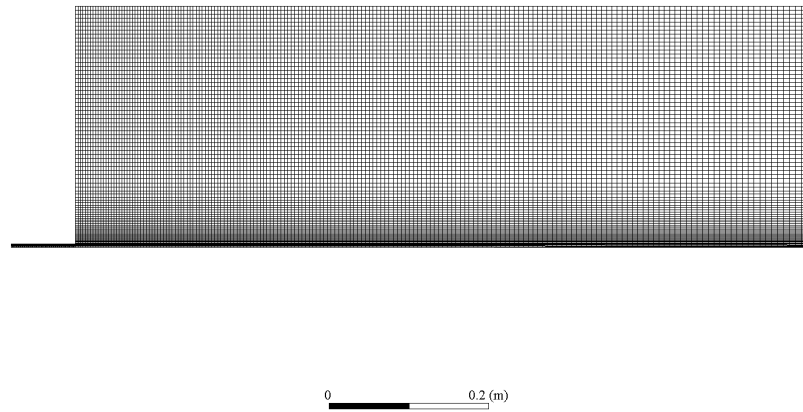


Figure 4.10: Overview of whole domain with fine mesh

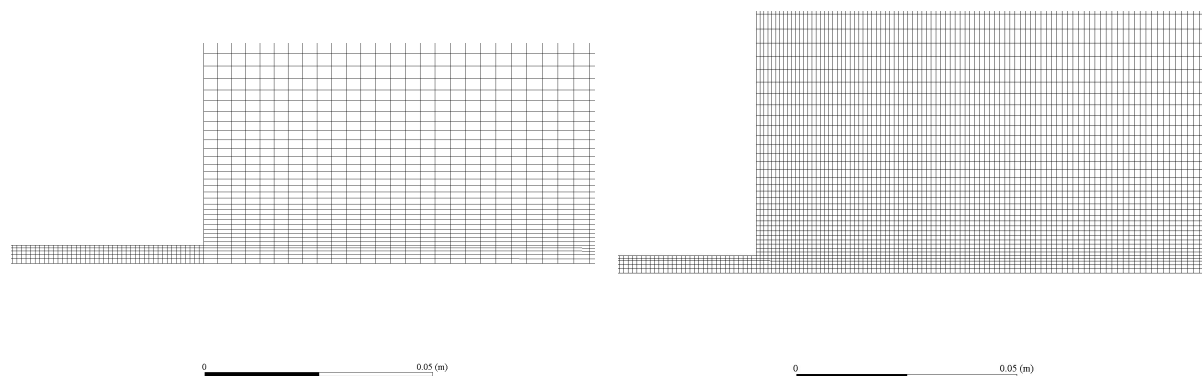


Figure 4.11: Mesh layout for both the fine mesh (left) and the very fine mesh (right)

4.2.3. Boundary Conditions

To ensure that the simulation will represent the experiment, the right boundary conditions have to be chosen. Figure 4.12 gives a visual representation of these boundary conditions.

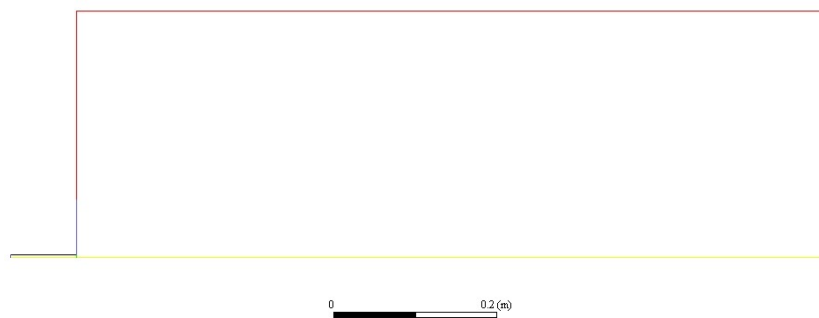


Figure 4.12: Overview of boundaries. Blue = inlet, Red = outlet, Yellow = symmetry and Black = wall.

Black is the wall of the fuel inlet and yellow is the axis of symmetry. The wall is assumed to have no-slip shear condition. The red lines represent outlets which are all modeled as constant pressure outlets. The inlets are blue where the larger one is the air inlet and the smaller one at the beginning of the pipe is the fuel inlet. As stated before the fuel is a mixture of 50% hydrogen and 50% nitrogen. The speed of air is 0.2 m/s and the speed of the fuel is 34.8 m/s. Both the inlets have a temperature of 298K. The prediction of the flow near the nozzle is very sensitive to the inflow boundary conditions if the inflow boundary is at the exit of the nozzle. This is true in RANS but even more so in LES. It is therefore recommended to start the flow domain sufficiently far upstream of the burner exit. To make sure that the fuel flow is fully developed and inflow boundary conditions

have less influence on the flow near the nozzle, it was chosen to make a long inlet of length $10 d$. A turbulent intensity was imposed at the beginning. According to the Ansys Fluent guide, the turbulent intensity can be estimated using Equation 4.1 [3].

$$I = 0.16(Re_{D_H})^{-1/8} \quad (4.1)$$

For the case of the H3 flame, which has a Reynolds number of 10,000, this would mean that the turbulent intensity should be equal to 5%. Figure 4.13 shows the results of varying the boundary condition of the turbulent intensity of the fuel. It can be seen that the recommended 5% gives a low kinetic turbulent energy at low heights, and increasing this value results in higher energy at low heights. The speed however decreases when more turbulent energy is present. Intensities higher than 10% caused Fluent to converge slower and the results are not significantly better. It was therefore chosen to have the air inlet at the recommended 5% intensity while the fuel inlet has a 10% intensity. The hydraulic diameter in the case of a cylindrical pipe is equal to the pipe diameter.

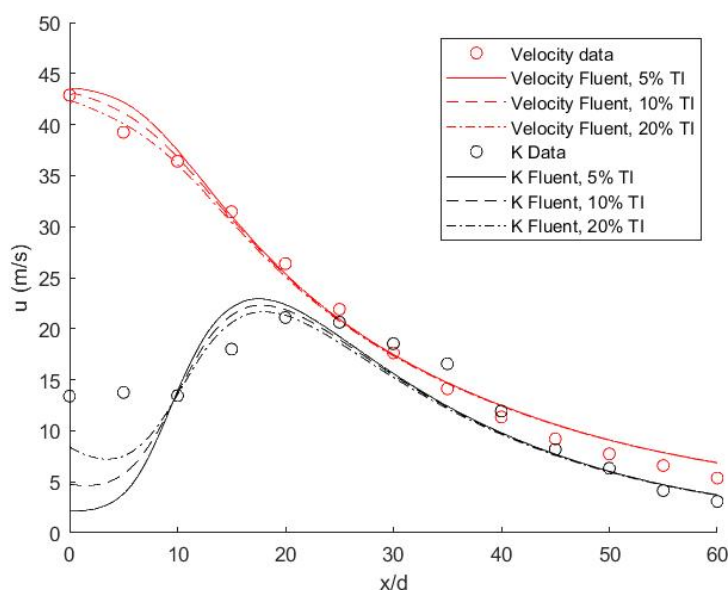


Figure 4.13: Turbulent kinetic energy and velocity along the centerline for various turbulent intensities (TI) using the chemical equilibrium model with the Li mechanism

4.2.4. Models

The goal of this research is to use the flamelet generated manifold model and include differential diffusion using this method. In order to do this and to see if this is effective, several other models will be used both for comparison and for validation. First the non-premixed chemical equilibrium model is used 4.3. Secondly, the steady flamelet model is used 4.4 and finally the flamelet generated manifold model is used 4.5. For all these models it is assumed that the flame is adiabatic and hence no energy model is used. It is also assumed that radiation will be very small and therefore radiation models are not used. This assumption was studied earlier by Pitsch et al. [34]. For turbulence the $k - \epsilon$ model is used. The different type of turbulence models and model constants will be evaluated using the chemical equilibrium model in Section 4.3.

The solution methods used by Fluent are as follows. The pressure-velocity coupling used the SIMPLE scheme. The gradient is evaluated using the least squares cell based method. The pressure is evaluated using the second order scheme and the momentum, Turbulent Kinetic Energy (TKE), turbulent dissipation rate, mean mixture fraction and mixture fraction variance are all evaluated using the second order upwind scheme. The solution controls are not changed from the basic Fluent settings, except for the mean mixture fraction and the progress variable if there is a convergence problem. Initialization is done from the air inlet and the calculation will run until the residuals are smaller than $1e-5$ or until the residuals are steady. If the latter is the case

it should be checked using contours and graphs that there is a steady case.

4.3. Chemical Equilibrium Model

The non-premixed chemical equilibrium model is used to determine which $k-\varepsilon$ model is to be used and if the constants of the model should be adapted for a better fit. The velocity and TKE will be used for this comparison. As the data does not include the TKE, it will be calculated using that k is half of the sum of the normal variances in speed (Equation 4.2 [30])

$$k = \frac{1}{2}(\overline{u'u'} + \overline{v'v'} + \overline{w'w'}) \quad (4.2)$$

The standard $k-\varepsilon$ model has a large deviation from the data, and hence the constants should be adapted to get a better fit. As stated by Pope [36] previous work has changed the constant $C_{\varepsilon 1}$ from 1.44 to 1.6 to get better results for round jets. This change resulted in a better fit. Both the standard and adapted results can be seen in Figure 4.14. The realizable $k-\varepsilon$ should in theory also be a good fit for the H3 flame and was also recommended by Fluent. However, the results were not as good as those for the standard $k-\varepsilon$ model. Even when $C_{\varepsilon 2}$ was changed from 1.9 to 1.8 they still differed more than the standard model, as can be seen in Figure 4.15. Therefore, the adapted version of the standard $k-\varepsilon$ model where $C_{\varepsilon 1}$ is changed from 1.44 to 1.6 will be used for all successive calculations.

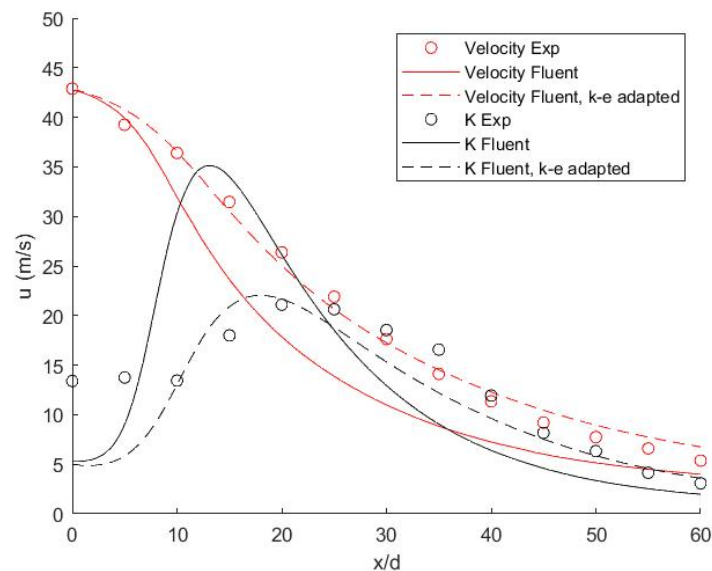


Figure 4.14: TKE and velocity along the centerline for standard and adapted standard $k-\varepsilon$ model

In order to validate the chemical equilibrium model and to see if it is a good base to build on with the next models, the velocity, mixture fraction, progress variable and temperature will be compared with the data. The velocity and TKE along the centerline have already been presented above. An error analysis was done at some positions along the centerline which can be seen in Table 4.1. The error for the velocity remains below 5% in the beginning and increases as the speed gets smaller. The maximum TKE error however is 60% and the error further downstream is below 20%. This large error at the inlet is mostly due to the turbulent boundary condition at the inlet which could not be increased any further without compromising the error of the velocity and the convergence of the model. A cause of the large error could be that the assumption that the inflow is fully developed turbulent flow is wrong. The simulation was therefore done with a domain without a pipe inlet and with a flat inflow profile, but in this case the overall value of the TKE was lower and even though a better result was obtained at the inlet, the error was still 40%. The research from D'Ausilio et al. [13] also had a large error in their velocity rms results. They stated that the numerical rms values (which are used to calculate TKE) usually have a larger experimental uncertainty compared to the other values, which can also cause larger errors.

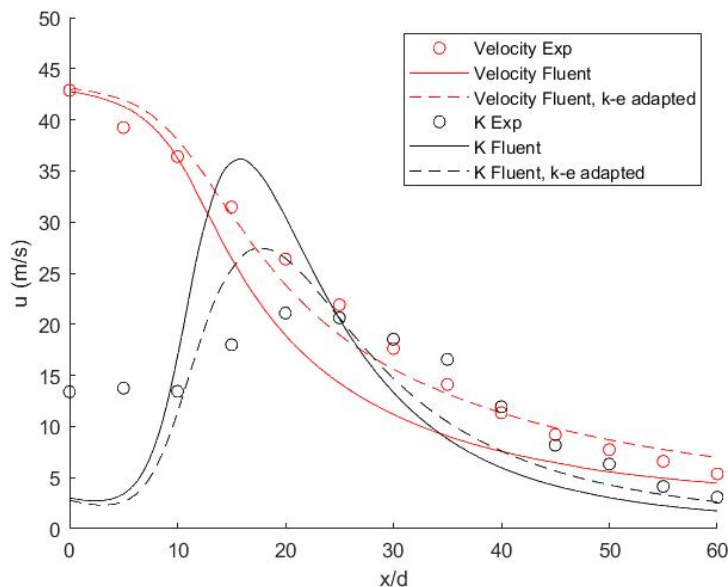


Figure 4.15: TKE and velocity along the centerline for realizable and adapted realizable $k-\epsilon$ model

x/d	u_{exp} (m/s)	u_{sim} (m/s)	u Err (%)	k_{exp} (m^2/s^2)	k_{sim} (m^2/s^2)	k Err (%)
5	39.3	40.7	3.6	13.8	5.8	-58.0
10	36.4	36.5	0.3	13.4	13.0	-3.0
20	26.3	25.0	-4.9	21.1	21.6	2.4
30	17.6	17.2	-2.3	18.5	15.3	-17.3
40	11.4	12.3	7.9	11.9	9.6	-19.3

Table 4.1: Error analysis of velocity and k along the centerline

The radial profiles of the velocity are shown in Figure 4.16. They are in good agreement with the data, both close to the nozzle and further downstream. The same can be said for the radial profiles of the mixture fraction which can be seen in Figure 4.18. The temperature however (also Figure 4.18) differs quite a lot from the data. The initial peak that the data shows close to the nozzle is 600K higher than the one calculated by Fluent. As stated before the low temperatures close to the nozzle are something that has been observed many times and is probably caused by not including differential diffusion and the limitation of the chemical equilibrium assumption (infinitely fast chemistry). Moving further downstream the temperature has a better match at $x/d=20$ but differs more at $x/d=40$. This can also be seen in the radial temperature profile in Figure 4.19. The data and simulation are in good agreement until the maximum temperature is almost reached. After that, it can be seen that the temperature peak in the simulation has shifted and that the temperature remains too high in the lean part of the flame. Both the mixture fraction and the major species (Figure 4.17) also agree with this, the agreement is good for the rich part of the flame but not on the lean part. Pitsch et al. [34] have done simulations in Fluent for the H3 flame with the same Pope correction and using the steady flamelet model and encountered the same phenomena. According to them the shift is caused by underprediction of the spreading rate which can cause the flame length to be too long and the maximum temperature location to shift. They also state that the overprediction on the lean part is due to the use of the $k-\epsilon$ model and can be reduced using the RSM. As this research mainly focused on the flame close to the nozzle it is not useful to switch to the RSM.

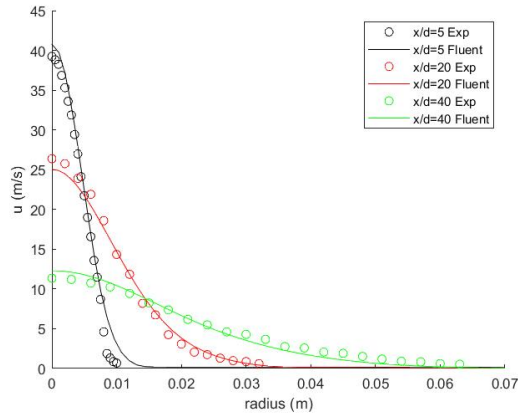


Figure 4.16: Radial velocity profiles at various locations

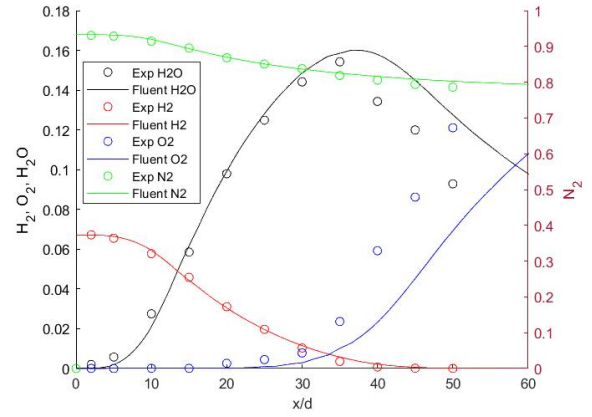


Figure 4.17: Major species along the centerline

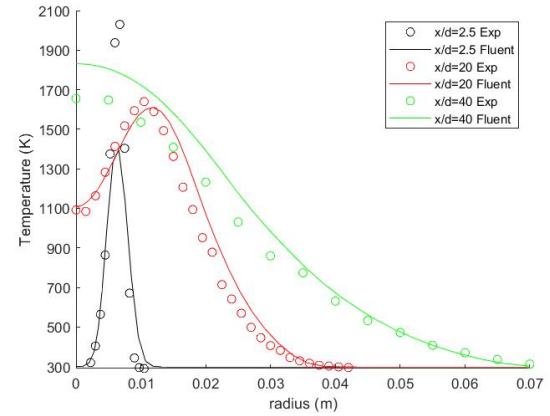
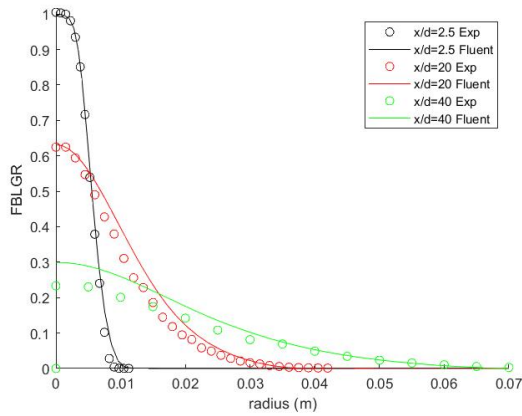


Figure 4.18: Radial profiles of mixture fraction (left) and temperature (right) at various locations

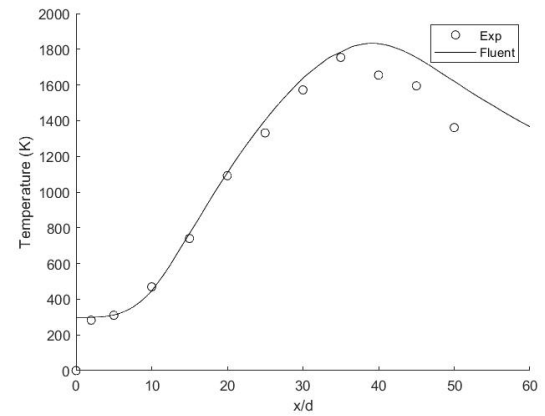
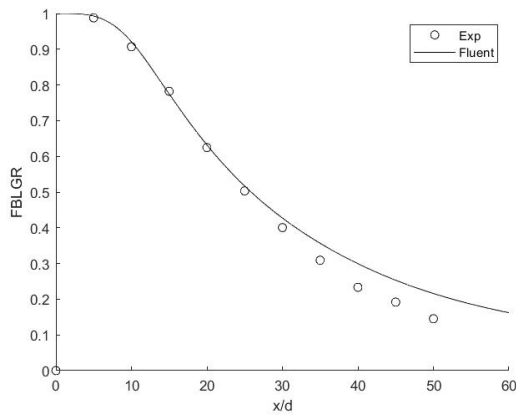


Figure 4.19: Mixture fraction (left) and temperature (right) along the centerline

4.4. Other Fluent Models

In order to see if there are other options in Fluent besides using the FGM in combination with the UDF, both the steady diffusion model and the standard FGM model have been considered.

4.4.1. Steady Diffusion Model

The steady diffusion model was interesting to use because it offers the option to import flamelets. By this is meant that laminar flamelets are imported and the PDF integration is done in Fluent. The results for the

steady diffusion model without importing flamelets were almost the same as the chemical equilibrium model. The graphs on the left in Figures 4.20, 4.21 and 4.22 show some of the results. To try and start including some of the flamelets with differential diffusion created by CHEM1D, the option to import flamelets was explored. Fluent did recognize the imported flamelets and the representation of these in figures of tabulated data was good. However, when the PDF table was constructed from these flamelets it showed no variations in terms of temperature and was therefore unusable. When running this simulation no combustion would take place.

4.4.2. FGM Model

The other model that was explored was the FGM model. The first simulation was done using the standard FGM with flamelets created by Fluent. The results can be seen in Figures 4.20, 4.21 and 4.22 on the right side. Once again, the results are almost identical to the results of the chemical equilibrium model. The next step was to import the FGM created by CHEM1D as a flamelet. This time the PDF table did show results but not above 880K. There were also some warnings which were due to the fact that the Fluent FGM model would only work in partially premixed combustion but the created FGM was non-premixed combustion. As the warnings could not be resolved this simulation would not give valid results. The trends in the graphs were the same as in the default FGM, just with lower values.

It can be concluded that when the flamelets are created by Fluent, both the steady diffusion model and the standard FGM model give results identical to the chemical equilibrium model. Importing flamelets could be a useful tool, but it needs to be improved to get good results in the case of a non-premixed flame.

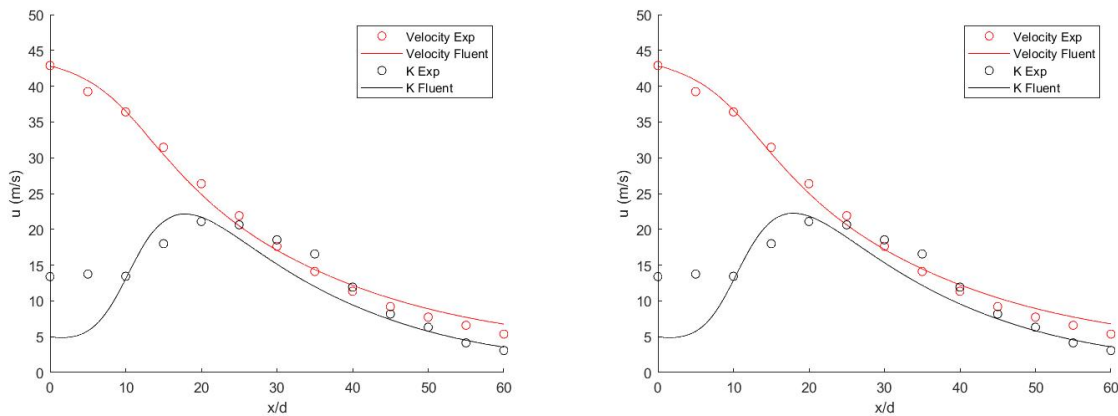


Figure 4.20: TKE and velocity along the centerline for steady flamelet model (left) and standard FGM model (right)

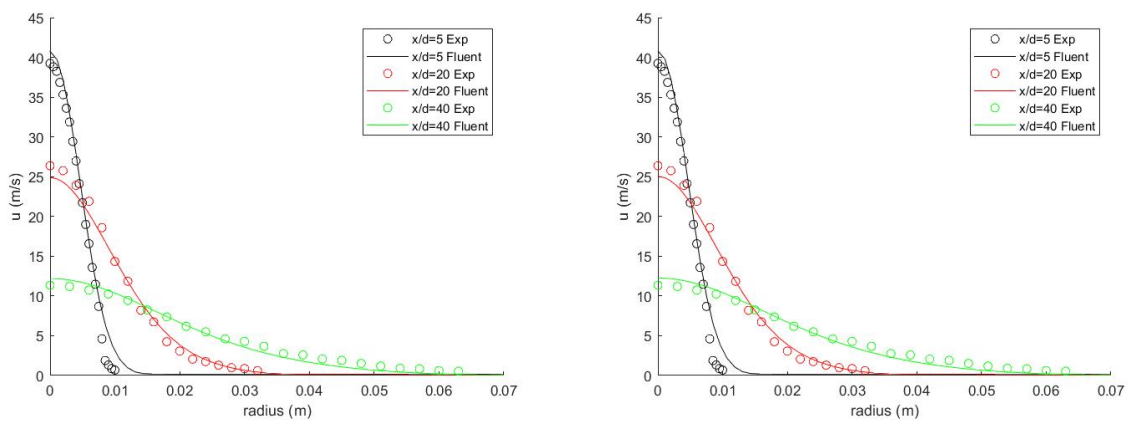


Figure 4.21: Radial velocity profiles at various locations for steady flamelet model (left) and standard FGM model (right)

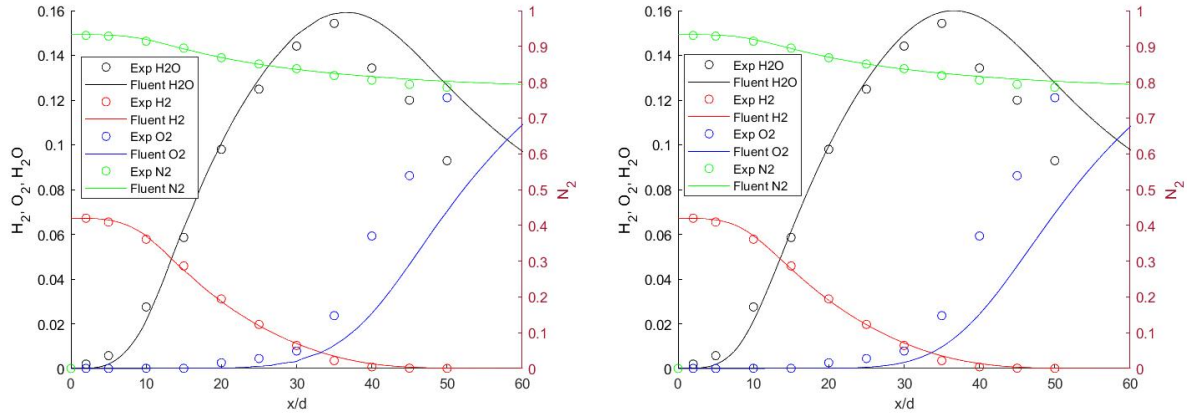


Figure 4.22: Major species along the centerline for steady flamelet model (left) and standard FGM model (right)

4.5. Flamelet Generated Manifold model with UDF

The simulations in this section are done using the UDF as created by Mengmeng Ren [39] which was adapted from the UDF by Naiara Romero-Anton [42]. The UDF itself was not changed but some changes were made in the Matlab files which create the PDF integrated tables used in the UDF. The UDF can also be found in Appendix A. It uses the PDF integrated table obtained from the previously created FGM and creates a PDF integrated table which can be read by Fluent which includes the following properties: density, mean mass, specific heat, temperature, source PV and the minimum and maximum values of the PV. Because the table created by the UDF overwrites the table from Ansys Fluent, there are limitations on which properties can be included in the table. A disadvantage of this is that the mass fraction of the different species is not calculated and can therefore not be compared to the data. Another disadvantage is that due to the lack of species in the UDF the more recent versions of Fluent give an error when trying to run a simulation. For future simulations it would be good to see if more properties could be included in the table for more extended analysis. Table 4.2 gives an overview of which FGM methods were used and what the differences between these are.

	Flamelet calculation	PDF integrated table	Differential Diffusion
Method 1 (Section 4.4)	Fluent	Fluent	No
Method 2 (Section 4.4, fails)	CHEM1D	Fluent	Yes
Method 3 (Section 4.5)	CHEM1D	CHEM1D (UDF import)	No
Method 4 (Section 4.5)	CHEM1D	CHEM1D (UDF import)	Yes
Method 5 (Section 4.5)	CHEM1D (different chemistry)	CHEM1D (UDF import)	Yes

Table 4.2: Overview of FGM methods used

4.5.1. Unity Lewis Numbers

The first model using the UDF that will be discussed is the one where differential diffusion is not yet included. The settings of CHEM1D are the same as for the one with differential diffusion, but the Lewis numbers that are used are equal to 1. The results of this model should approximately be the same as the results for the models previously described as these also do not include differential diffusion and use the same chemical scheme. When running this simulation, a numerical oscillation occurred in the flame, which made it hard to converge. The solution controls (relaxation factors) for the progress variable and mixture fraction were therefore lowered to 0.5 to get a steady jet flame.

The results were as expected. The velocity and mixture fraction profiles are the same as the previous simulations. The progress variable and temperature profiles are slightly different. The un-normalized progress variable can be seen in Figure 4.23 and the temperature graphs are shown in Figure 4.24. The agreement with

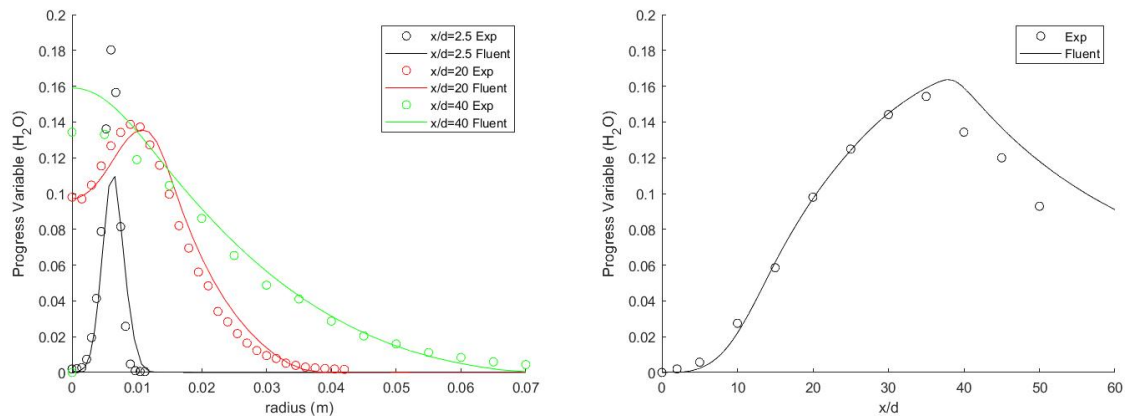


Figure 4.23: (Un-normalized) Progress Variable at different positions (left) and along the centerline (right).

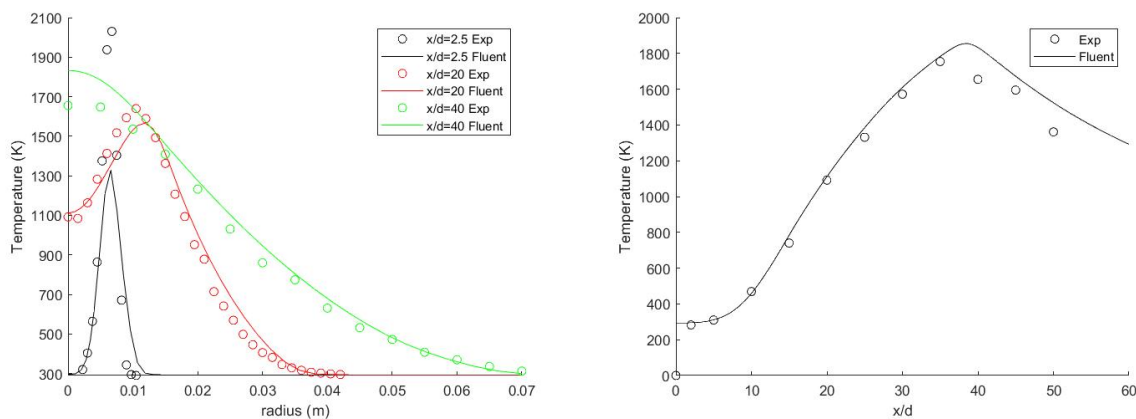


Figure 4.24: Temperature at different positions (left) and along the centerline (right)

the data is the same as before although the peak in progress variable and therefore temperature close to the nozzle is slightly lower. The shift of the maximum temperature to a location more downstream can still be seen. As the agreement with the data is still good and almost the same as with models created by Fluent itself, it can be concluded that the UDF is working properly and including differential diffusion is the next step.

4.5.2. Non-unity Lewis Numbers

Here the UDF model including differential diffusion will be discussed. The actual Lewis numbers were used in CHEM1D in order to include the diffusion of all the species. Although the PDF integrated table has a lot in common with the unity Lewis PDF integrated table (as can be seen in Section 4.6) there were some problems regarding the convergence of the model. Just like the unity Lewis model, the methods and controls had to be changed to get a better convergence. However, in this specific case the residual associated with the progress variable called premixc, converges for a bit but then goes up to a value in the order of $1E01$ and stays constant for the remainder of the calculation. Using different controls will cause the residual to be slightly lower but it is not significant. A different turbulent model also did not cause this residual to converge. As the unity Lewis case gave good results using the same UDF and CHEM1D methods it can be concluded that the convergence problem probably has to do with the added differential diffusion. Even though the model did not converge fully, the results on the contours seemed like a steady state had been reached and the results are therefore still presented and discussed.

Figure 4.26 shows the contours of the flame which indeed show the expected steady flame. The velocity and mixture fraction were again in good agreement, but some unusual behaviour could be seen in the temperature and progress variable graphs. The un-normalized progress variable is shown in Figure 4.27. Close to the nozzle the progress variable performs better than for the other models, which means that the addition

of differential diffusion did influence the results. The same goes for the temperature, the temperature peak close to the nozzle is higher than for all of the previous models but there is still a difference of 400K. When moving away from the nozzle it can be seen that the profiles take an unexpected shape. Sharp points occur in the profiles, especially for the temperature.

There are several reasons why these profiles could take these shapes. First of all it can be because of the content of the PDF integrated table. Fluent retrieves data from the created PDF tables and if there is a gap between two datapoints it can show up as a sharp gradient. If this is the case a table with more datapoints can be the solution. A new table was created with 21 instead of 11 mixture fraction- and progress variable variance points. Using this refined table in Fluent did not give different results. Secondly, sharp points can mean that the spatial mesh is not fine enough. A new mesh was created with 56,848 cells instead of 31,312 cells. The new mesh resulted in a higher computational time but did not resolve the peaks. Another thing that was noticeable and could be the cause was the contour of the un-normalized progress variable variance. Figure 4.25 shows that small spots occurred which might be due to the lack of convergence. One of the measurement lines is at $x/d=20$ which is also shown in the contour. It crosses straight through one of these spots and even though the variance is very small it might cause the peak. To check this radial profiles were considered right before and after this spot. These measurements also showed sharp peaks in their profiles and hence this was also not the cause. The lack of convergence mentioned before can of course also be the cause of the profile, even though the contour shows a steady flame. Finally, it was hypothesized that the sharp peaks could be due to the chemical scheme used. Another scheme might give other results. This will be further discussed in the next section.

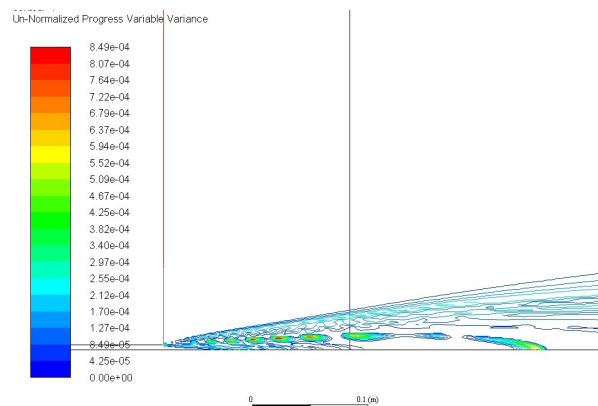


Figure 4.25: Un-normalized Progress Variable variance contour with a super imposed line at $x/d=20$

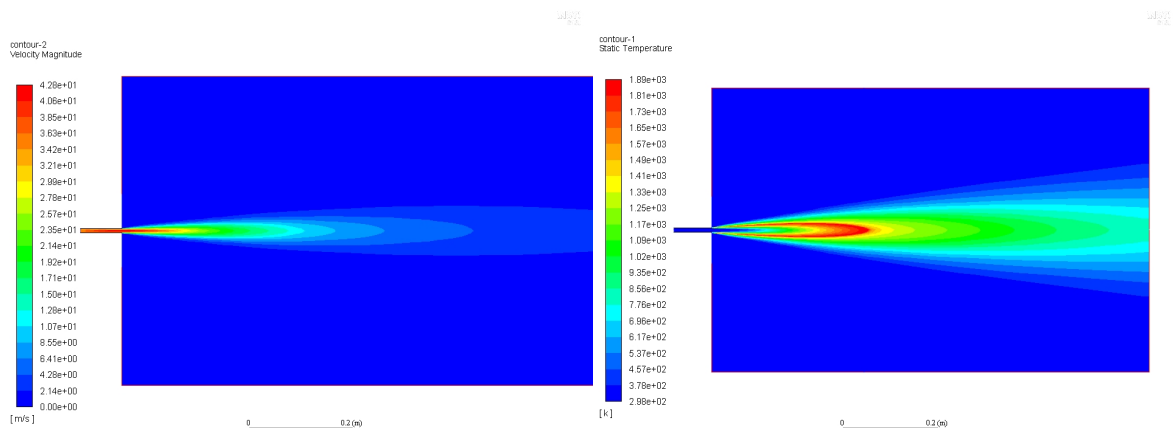


Figure 4.26: Contour of the velocity (left) and the temperature (right)

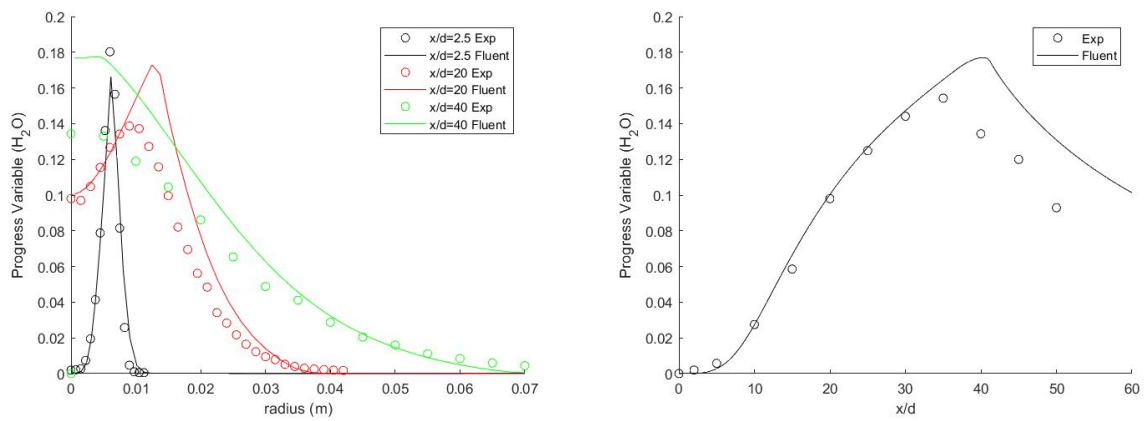


Figure 4.27: Un-normalized Progress Variable at different positions (left) and along the centerline (right).

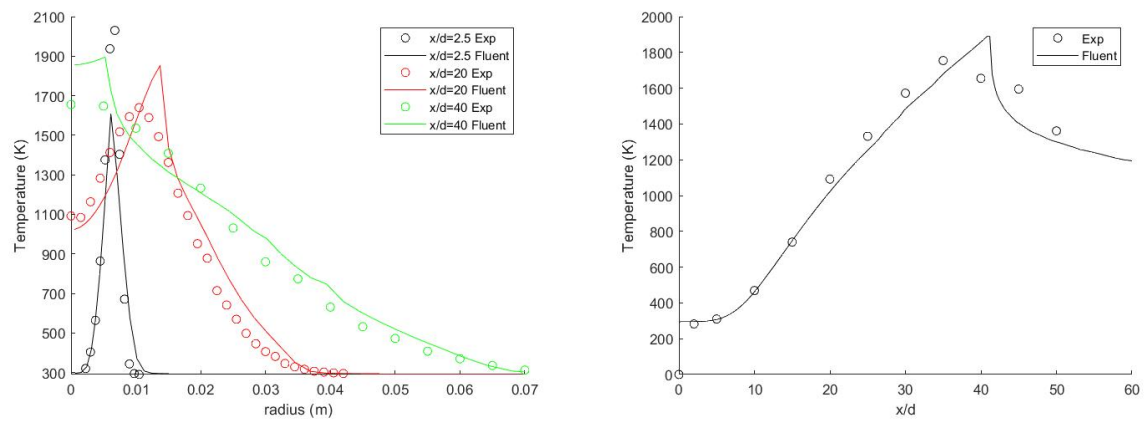


Figure 4.28: Temperature at different positions (left) and along the centerline (right)

4.5.3. Sensitivity to Chemical Model

In the previous section it was hypothesized that changing the chemical model might lead to a better converging model. Next to the model by Li et al. [22], two other chemical models have been used. The first one is by Burke et al. [6] which is based on the mechanism by Li et al. The second is from the ELTE university [27] which was based on a mechanism with 15 species and 44 different reactions. For all of these mechanisms, an FGM was created using CHEM1D. Contour plots of the progress variable source term are shown in Figure 4.29. The shape of the high activity region is a heart in all of the graphs, which is probably due to the effect of scaling the progress variable. On the top the graph for the Li mechanism are shown where the left side is for different Lewis numbers and the right side with unity Lewis numbers. The one with different Lewis numbers has a higher source term PV and is located at a mixture fraction of 0.2 instead of 0.3. When comparing the graphs on the bottom with different mechanisms, it can be seen that the ELTE mechanism gives almost identical results to the Li mechanism, but the Burke mechanism has a slightly lower source term PV. To see if the lower source term PV can help with convergence, a simulation was done using the Burke mechanism.

The new chemical mechanism did not give results that were significantly different from the results obtained using the Li mechanism. Figure 4.30 shows the temperature plots for both mechanisms. It can be concluded that there is almost no difference between the two. The chemical mechanism is therefore not the reason for the sharp peaks that have been observed in some of the graphs.

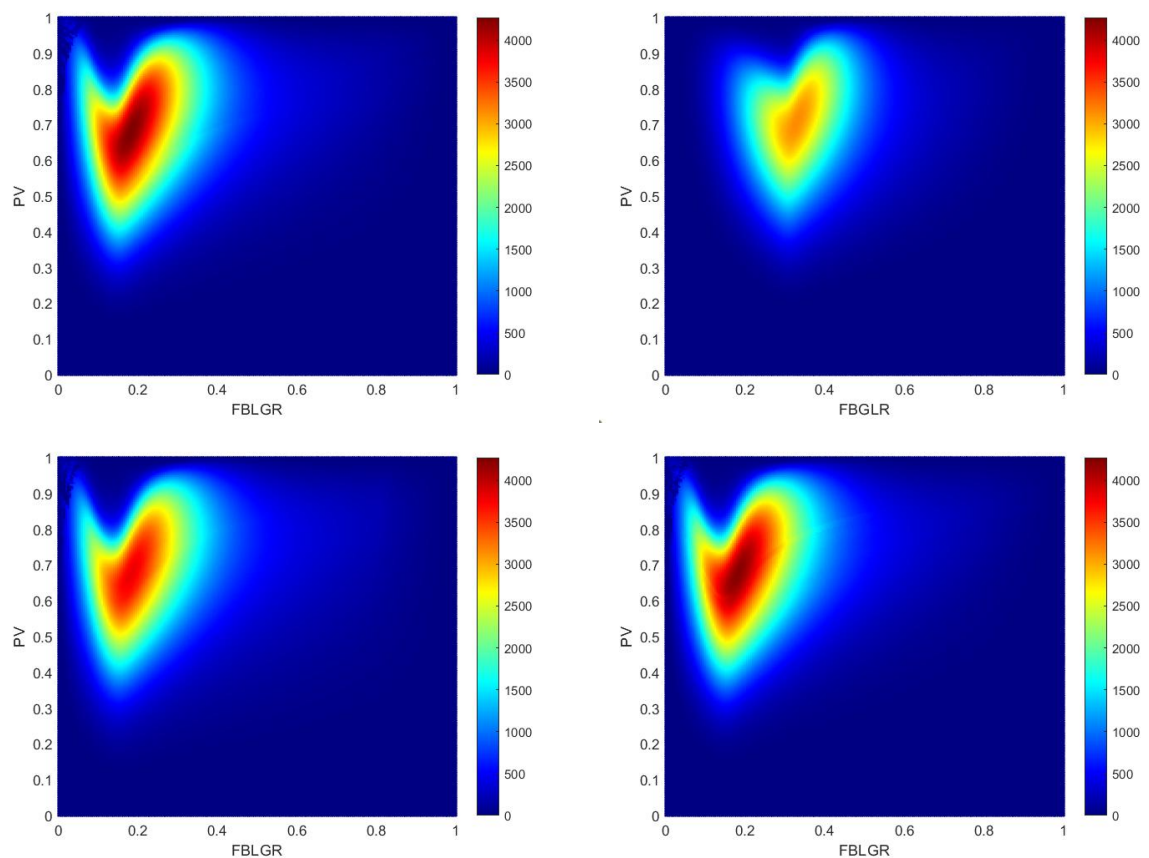


Figure 4.29: Progress variable vs mixture fraction where the color represents the progress variable source term. Mechanisms used are by Li et al. [22] with DD (top left), Li et al. without DD (top right), Burke et al. [6] with DD (bottom left) and a mechanism by ELTE with DD [27] (bottom right)

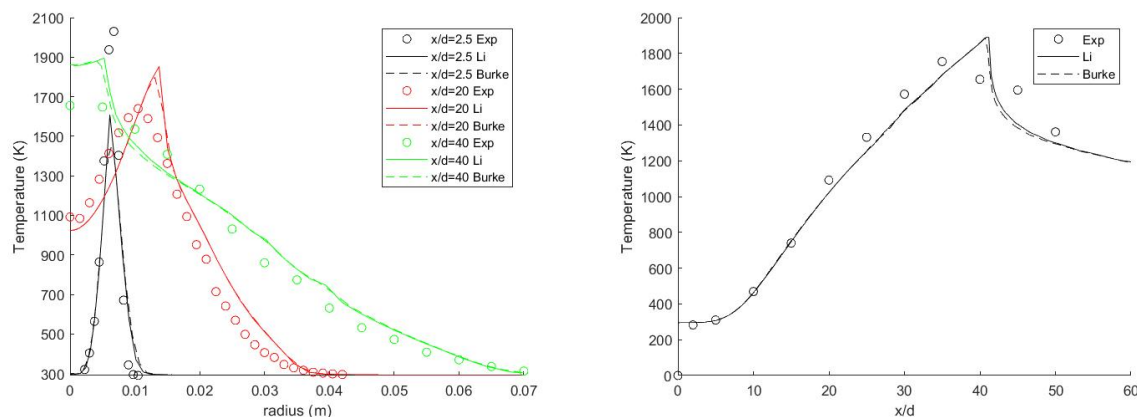


Figure 4.30: Comparison of the Li mechanism and the Burke mechanism for the temperature at various positions (left) and along the centerline (right)

4.6. Model Comparison

Several simulations were done and their results will be discussed in this section. As a lot of models gave similar results it was chosen to compare one of the standard Fluent models, chemical equilibrium, to the two models that used the UDF, one with actual Lewis numbers and one with unity Lewis numbers. Since there were some differences in converging for the two UDF models, the values in the integrated PDF tables are compared to see if there are noticeable differences that could lead to these problems. They can be found in Figure 4.31 and 4.32. It can be seen that the overall shape is the same. Both tables have more scattered data points for a high source PV. One difference is that the actual Lewis number table reaches higher values of both temperature and source term PV. This was however why the actual Lewis numbers were used, to reach higher temperatures. The other main difference is that the location of the peak with respect to the mixture fraction is shifted to the left compared to the unity Lewis model, which has a peak around the stoichiometric mixture fraction. It might be the case that the shift in stoichiometric ratio is the cause of the lack of convergence, but it is more probable that the higher source term value is the cause. This however needs to be researched.

To evaluate the results a comparison of the models is made. Firstly, the velocity and mixture fraction results are shown in Figure 4.33. All models show good agreement here with the data and each other, the only thing is that all of them slightly overpredict the mixture fraction at the center around $x/d=40$. In Figure 4.34 the temperature profiles are shown, which have been split up into two figures for clarity. One of the main goals of this research was to get a better representation of the temperature at the inlet by including differential diffusion. It can be seen that the model with actual Lewis numbers does perform better compared to the other two at $x/d=2.5$, but there is still a large difference between the experimental data and the simulation. The peak temperatures are accessible using the FGM as they are presented in the flamelets but in the presence of large fluctuations in the mixture fraction and/or progress variable this peak would no longer appear in the predictions for mean temperature. Therefore, it is a possible hypothesis that the underprediction of the peak in the mean temperature is due to an overprediction of the level of fluctuations. In the RANS model this is controlled by the modelled equations for the variance of mixture fraction and progress variable. Checking agreement of variance of the mixture fraction and progress variable with experimental data would provide useful information to check the hypothesis. An error analysis of the maximum flame temperature can be seen in Table 4.3. It can be concluded that the model including differential diffusion does give better results when looking at the maximum flame temperature. The model with differential diffusion also still develops higher temperatures later on. It could be the case that due to the shift in stoichiometric ratio in the DD FGM that the higher temperatures occur at a different position, which could mean that the maximum flame temperature is reached, just not at the right position. It could also be the case that the boundary condition needs some improvement which can lead to the flow developing earlier. Table 4.4 contains an error analysis of the maximum flame temperature position. It can be seen that the error gets bigger when one moves further downstream. Note that for the simulation a lot of the maximum flame temperature positions are the same, which is due to the fixed step size between data points that Fluent uses when data is exported. Figure

4.35 shows the comparison of the un-normalized progress variable. The radial profiles coincide except for the profile with DD, which was also seen in the temperature graphs. One reason for this could be that in the experimental data differential diffusion is mostly suppressed, so in the case of the FGM the differential diffusion might be too strong and cause results downstream to be too high.

x/d	T_{exp} (K)	$T_{sim,CE}$ (K)	$T_{sim,noDD}$ (K)	$T_{sim,DD}$ (K)	CE Err (%)	no DD Err (%)	DD Err (%)
2.5	2030	1395	1328	1609	-31.3	-34.6	-20.7
10	1701	1525	1455	1712	-10.3	-14.5	0.6
20	1640	1610	1566	1853	-1.8	-4.5	13.0

Table 4.3: Error analysis of maximum flame temperature

x/d	r/d exp	r/d sim, CE	r/d sim,no DD	r/d sim, DD	CE Err (%)	no DD Err (%)	DD Err (%)
2.5	0.85	0.83	0.83	0.76	-2.9	-2.9	-10.3
10	1.13	1.20	1.20	1.20	6.7	6.7	6.7
20	1.31	1.49	1.49	1.71	13.3	13.3	30.5

Table 4.4: Error analysis of maximum flame temperature location

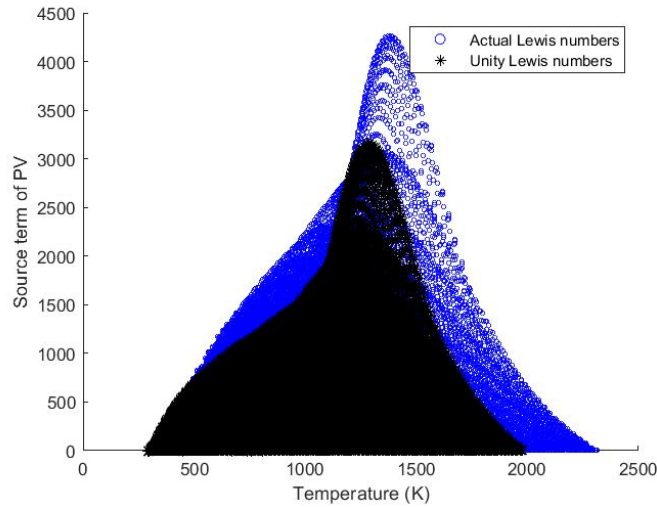


Figure 4.31: Source term of PV vs temperature for 2 different PDF integrated tables

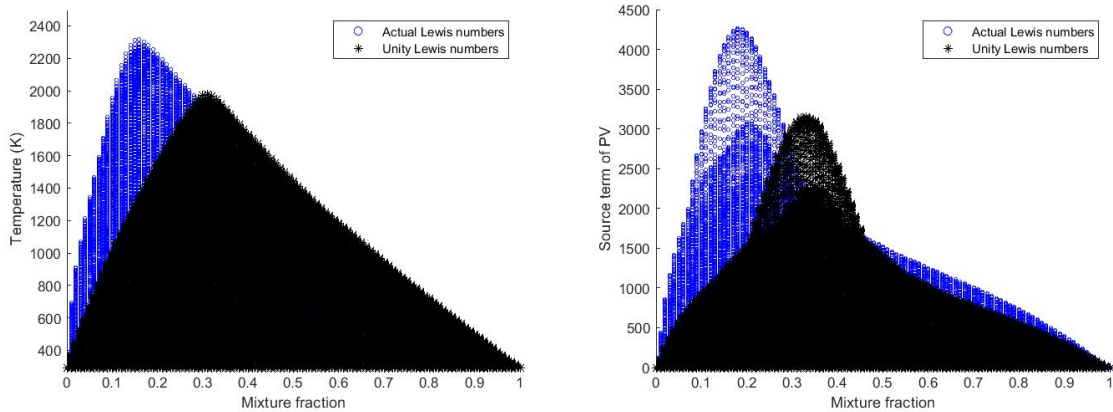


Figure 4.32: Mixture fraction vs temperature (left) and mixture fraction vs source term of PV (right) for 2 different PDF integrated tables

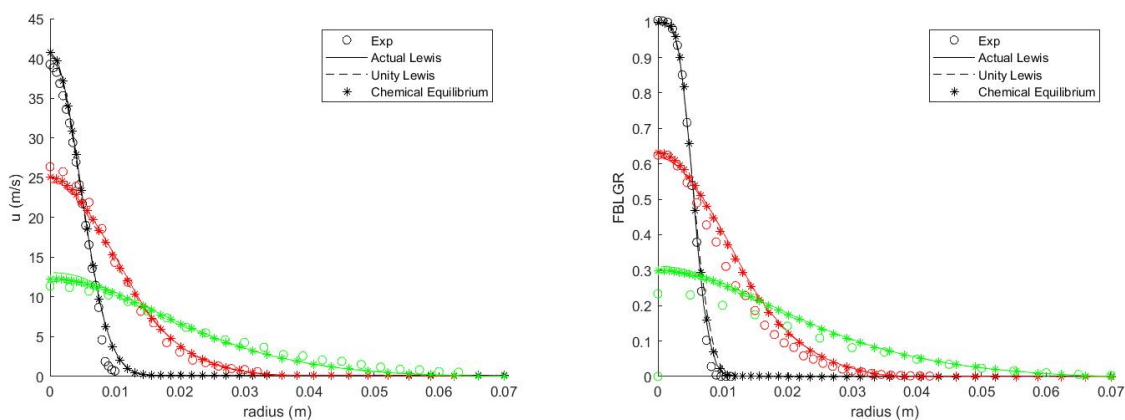


Figure 4.33: Velocity (left) and mixture fraction (right) at different positions. Black is measured at $x/d=5$ (velocity) and $x/d=2.5$ (FBLGR), red is measured at $x/d=20$ and green is measured at $x/d=20$.

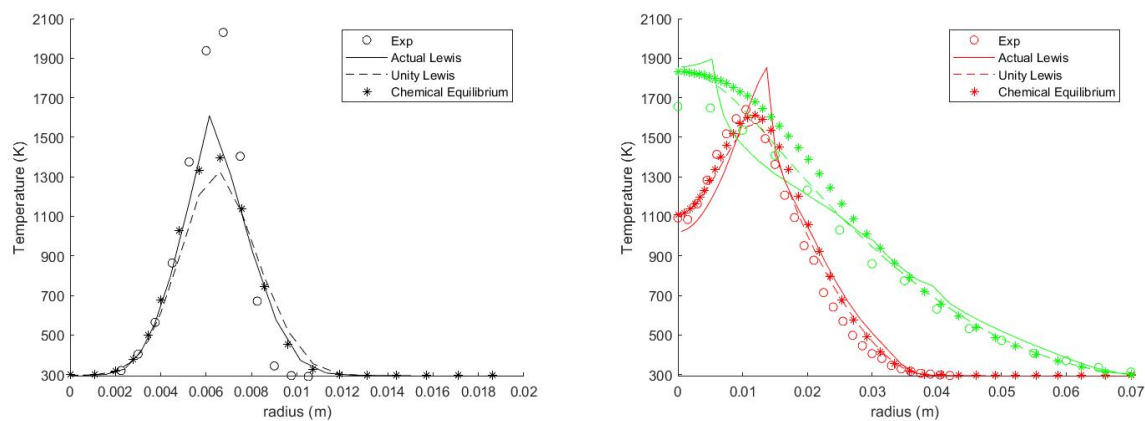


Figure 4.34: Temperature at $x/d=2.5$ (left) and at $x/d=20$ (red) and $x/d=40$ (green) (right)

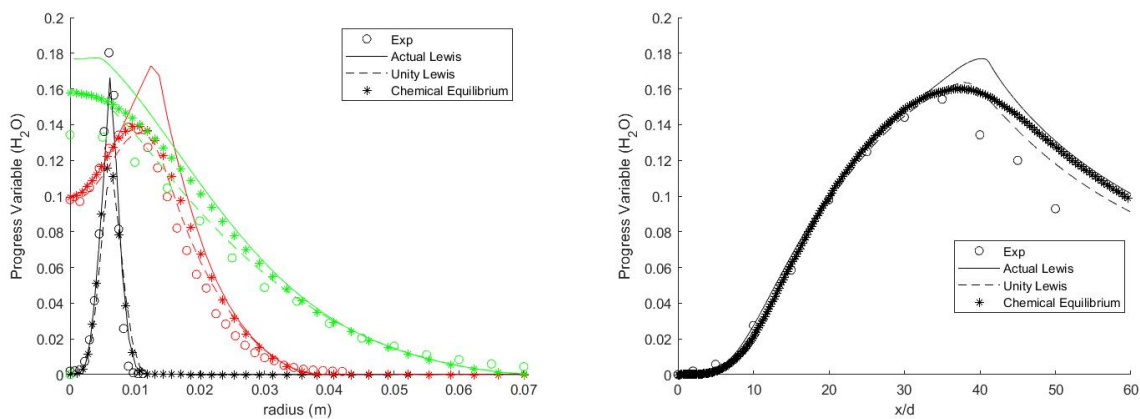


Figure 4.35: Un-normalized progress variable at different positions (left) and along the centerline (right)

4.7. Comparison to previous research

A lot of simulations have been done using the H3 flame. This section will shortly talk about previously obtained results and how they compare to the simulations done in this research. The best way to compare the results is by plotting them in the same figure, but due to different ways of processing the data and calculating the means this was not possible without compromising results. Therefore the results are shown separately and a comparison table has been made.

Table 4.5 shows the key characteristics of the four simulations that are compared. The simulation by d'Ausilio et al. [13] stands out by using LES, a full chemical mechanism and an advanced turbulence chemistry model (CMC). However, it did not include the effect of differential diffusion. The LES of Maragkos et al. [24] and d'Ausilio et al. both use a relatively simple method for representing turbulence at the inlet and furthermore the inlet boundary is at the fuel pipe exit and therefore very close to the region where differential diffusion has been observed in the experiments.

The work of Maragkos has the strong point of being a LES, but used only one step chemistry. This means that the differential diffusion only describes the differential diffusion of hydrogen in a mixture of hydrogen, nitrogen, oxygen and water. The present method used RANS, but by using a calibrated model constant, the profiles of mean velocity and mean mixture fraction are predicted to sufficient accuracy in order to address questions concerning properties in the flame front.

The discussion on presence of differential diffusion effects concerns the radial profiles close to the burner exit. Maragkos et al. noticed a significant difference between the simulation with and without differential diffusion taken into account. But, as mentioned, the simulation used one-step chemistry and therefore did not represent the differential diffusion effects in the real multicomponent mixture accurately.

In the present study differential diffusion is taken into account in the calculation of the flamelets. It makes the assumption that the flamelet structure itself is not destroyed by turbulence. This is reasonable for the case of hydrogen chemistry which is very fast. Pitsch et al. [34], using flamelet model, only report radial profiles at $x/d=20$ and $x/d=40$ of which the first one can be seen in Figure 4.19. The peak temperature is in good agreement, comparable with the unity Lewis number result of this work. But they predict a too broad flame.

Some of D'Ausilio's results are shown in Figure 4.36. Overall the results for D'Ausilio and the unity Lewis case in this research are in agreement. There are some small differences but this is to be expected as their model is more advanced. The results from Maragkos are shown in Figure 4.37. What is interesting is that their results without differential diffusion are very different from the ones with differential diffusion, which was not the case using the FGM model. Their model including one step chemistry and differential diffusion however overpredicts the temperature at the nozzle and is in good agreement further downstream, which was not the case in this research. It can be concluded that the velocity and mixture fraction results in this RANS work are comparable to the LES results.

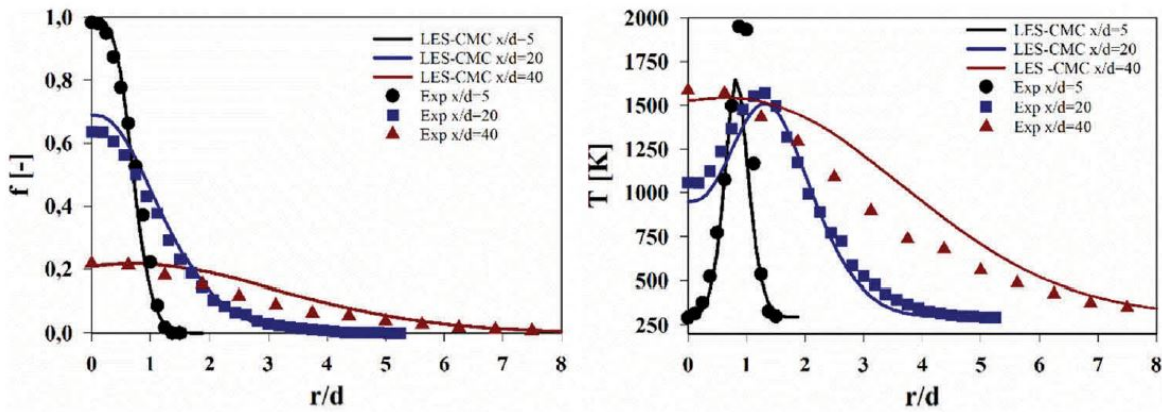


Figure 4.36: Mixture fraction (left) and temperature (right) at various locations by D'Ausilio et al. [13]

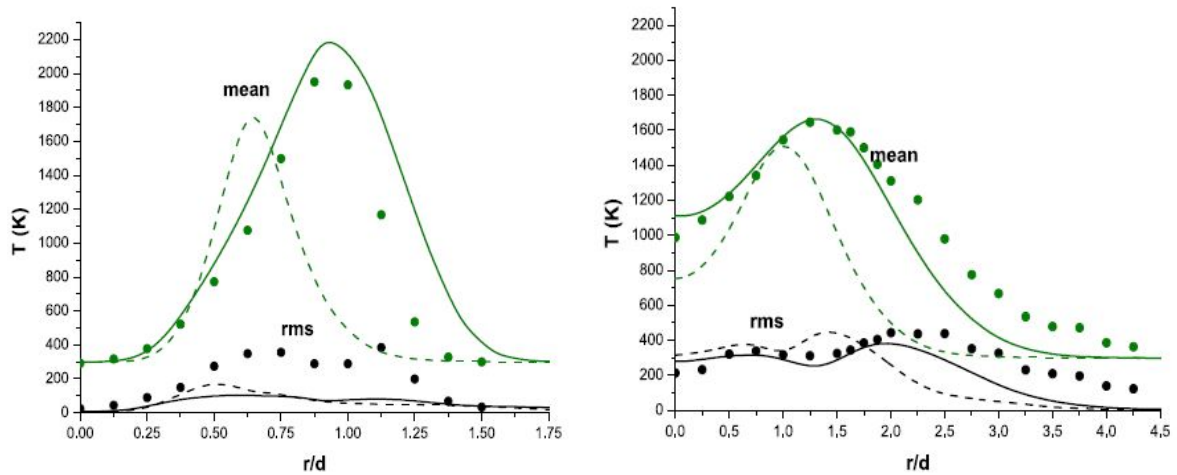


Figure 4.37: Temperature at $x/d=5$ (left) and $x/d=20$ (right) where the symbols are experimental data, the solid lines include differential diffusion and the dotted lines do not, by Maragkos et al. [24]

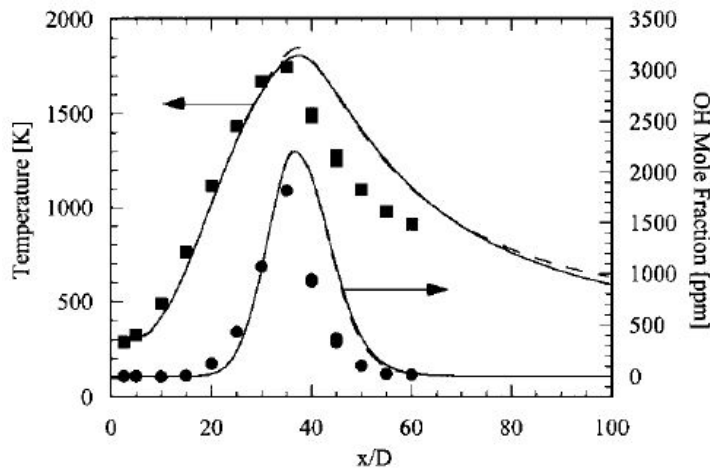


Figure 4.38: Temperature along the centerline by Pitsch et al. [34]

	Pitsch 1998 [34]	Maragkos 2015 [24]	D'Ausilio 2018 [13]	This work
Domain type	2D	3D	3D	2D
Axial-radial	100dx50d	65dx22d	81.25dx18.75d	125dx37.5d + inlet
Grid size	191x77	444,000	688,000	31,312
Platform	Fluent FlameMaster	OpenFOAM Modified FireFOAM 1.6 solver	ReactingFOAM Inhouse CMC Code	Fluent 18.2 + UDF CHEM1D
Turbulence	RANS	LES	LES	RANS
Closure model	$k - \epsilon$ with round jet correction	Dynamic one equation model	Dynamic one equation model	$k - \epsilon$ with round jet correction
Kinetic scheme	40 rev. reactions for 16 species (incl NOx)	One step Burke-Schumann	Li et al (2004), 19 reactions for 9 species	Li et al (2004), Burke et al (2011)
Turb-chem interaction	Flamelet 1. steady 2. unsteady 3. unsteady coupled to CFD	Presumed β -pdf for the two scalars. Variances from scale similarity	Conditional Moment Closure	FGM presumed β -pdf for two scalars
Thermochemical Scalar equations	Mean and variance of mixture fraction. Mean of enthalpy	Two conserved scalars (element mass fractions of H and N)	Conditional averages of species mass fractions	Mean and variance of mixture fraction and progress variable
Differential diffusion	Not included	Included and not included compared	Not included	Included and not included compared
Radiation	Without and with (emission only) are compared	Not included	Not included	Not included
Inflow BC's	Mean velocity: 1/7 power law	Velocity rms 3% (white noise)	Random spot method	At start fuel pipe 10% turb intensity

Table 4.5: Key characteristics of four simulations

4.8. Statistical Dependence

In the FGM approach the evolution of the local thermochemical state is assumed to follow the evolution on the manifold which is described by two independent variables, mixture fraction and progress variable. In the case of application of the FGM to a turbulent flame the influence of the turbulent fluctuations of the independent variables has to be taken into account. To do so the joint one-point PDF of mixture fraction and progress variable must be known. Then the mean quantities in the turbulent flow can be obtained by integration over all possibilities with the PDF as weight factor, for example

$$\tilde{Y}_k = \int_0^1 \int_0^1 Y_k^{FGM}(z, c) \tilde{P}_{Zc}(z, c) dz dc \quad (4.3)$$

For simplicity most often and also in this work it has been assumed that fluctuations of mixture fraction and scaled progress variable are statistically independent. This is defined mathematically by the condition that the joint PDF can be written as the products of the PDF of each variable separately (the PDF of one variable for a system depending on more than one variable is called ‘marginal PDF’) [37].

$$\tilde{P}_{Zc}(z, c) = \tilde{P}_Z(z) \tilde{P}_c(c) \quad (4.4)$$

Then the expression for the averages takes the form.

$$\tilde{Y}_k = \int_0^1 \int_0^1 Y_k^{fgm}(z, c) \tilde{P}_Z(z) \tilde{P}_c(c) dz dc \quad (4.5)$$

The model is completed by the assumption that each marginal PDF has the form of a β -function, the value of which is fixed when average and variance are known. The values of the PDF can be different at each location because the mean and variance can be different at each location. The calculation of averages in this way has been used to create the four-dimensional tables, with mean and variance of mixture fraction and progress variable as independent variable. The availability of joint measurements of all main species and temperature in the experimental database allows to check whether the assumption of statistical independence is satisfied is not. In order to do so a check must be done considering all data in a small part of the domain because the assumption of statistical independence is valid locally.

Figure 4.39 shows 3000 data points along the horizontal cross section $x/d=10$. Note that the progress variable has been scaled with taking into account the minimal and maximal value of unscaled progress variable at each Z . The minimum can be taken to be zero but the maximum has to be determined. It is available from the calculated flamelets in the model and it would also be available from the experimental data. Due to experimental error in single point experimental data a factor of 0.95 is applied to the maximum data points. Proof that the two variables are not statistically independent can be given by evaluating the correlation coefficient. It is a necessary condition for statistical independence that the correlation coefficient is zero (Equation 4.6) [9].

$$\rho_{X,Y} = \frac{Cov(X, Y)}{\sigma_X \sigma_Y} \quad (4.6)$$

For the dataset in Figure 4.39, the correlation coefficient is equal to -0.64. Neuber et al. [29] also calculated the correlation coefficient for the H3 flame. They calculated the correlation at various locations and it can be seen that at almost every position they evaluated, it is not equal to 0. So it is very clear that the statistical independence of mixture fraction and scaled progress variable is not satisfied.

The fact that c and Z are not statistically independent, can be represented by a function defined as the ratio of the joint PDF to the product of the two marginal PDF's. This is known as the copula [7]. By definition the copula is 1 in case of statistical independence. It would be of interest to see whether analysis of the experimental data would provide sufficient information to propose a mathematical expression of the copula.

Even when the variables are not statistically independent, it can be of interest to see whether the assumptions on the shape of the marginal PDF's (β -function) are valid. From the scatterplot an experimental result for the marginal PDF of Z and the marginal PDF of c can be determined. Histograms of either Z or c are constructed from the scatter plot. The range from 0 to 1 of either Z or c is divided into 100 bins and the

number of data-points in each bin is counted. On the other hand the β -PDF was computed using the mean and the variance of the experimental dataset. The marginal PDF's from the experimental data and from the β -function assumptions are represented in Figure 4.39. It can be seen that even though Z and c are statistically dependent, the β -PDF assumption for the marginal PDF performs reasonably well. The general shape of the β -PDF is in agreement but the marginal PDF gives a larger probability at higher values of Z than the β -PDF. This can lead to inaccuracies in the results, especially around the nozzle. The β -PDF is a good assumption for overall agreement, but these discrepancies need to be taken into account when evaluating the results.

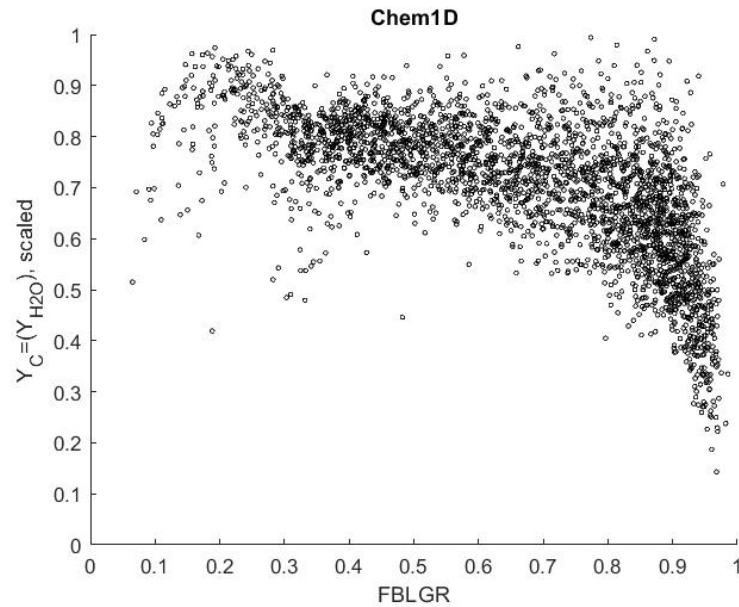


Figure 4.39: Scaled Progress variable vs mixture fraction for a data points at $x/d=10$

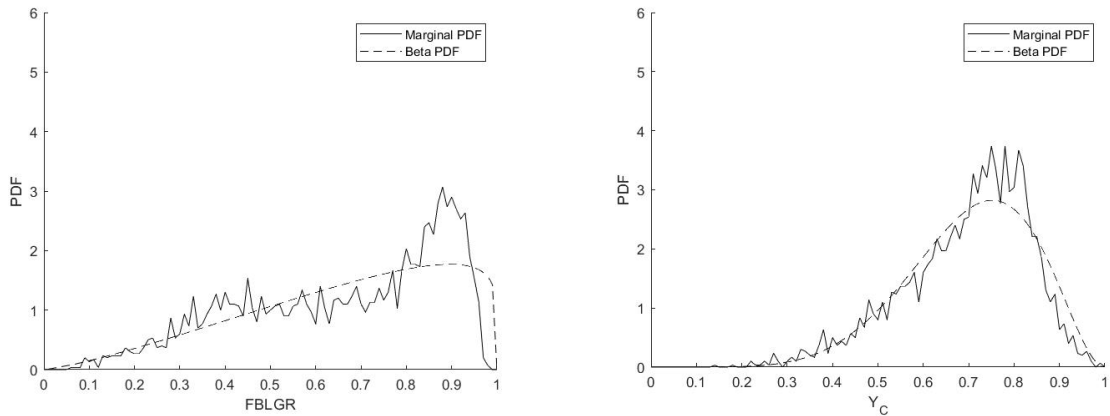


Figure 4.40: Comparison of marginal PDF and β -PDF for the mixture fraction (left) and scaled progress variable (right) at $x/d=10$

5

Conclusions and Recommendations

In this work a hydrogen flame was modelled using RANS methods with focus on including differential diffusion. First a comparative study was done between several turbulence and combustion models. From this it was concluded that the standard $k - \epsilon$ model with round jet correction and the FGM model were the most promising to use in combination with Fluent due to the existing UDF in combination with CHEM1D. In order to include differential diffusion, flamelets were created with the help of CHEM1D, a tool developed by TU Eindhoven. These flamelets were combined to an FGM table also including the effect of turbulence via a PDF and this table was imported into Fluent with the help of a user-defined function overwriting the default Fluent FGM table. The CHEM1D tool was used to create 3 different cases: one with Lewis unity numbers (no differential diffusion), one with actual Lewis numbers (differential diffusion) and another one with actual Lewis numbers but with a different chemical scheme.

The results of the chemical equilibrium model (which was used as a first validation model) and the model without differential diffusion were in good agreement with the data, except for the region close to the nozzle. Due to the $k - \epsilon$ model the flame is slightly too long and the temperature peaks start to shift further downstream. The model with differential diffusion gave acceptable results but has several issues. Firstly, there was a problem with the convergence of the progress variable variance in Fluent. Even though the flame seemed to be stable in the contours, this can cause inaccuracies. Sharp peaks could be seen in some of the profiles which can be due to this problem. Secondly, the stoichiometric ratio seemed to have shifted from 0.31 to 0.2 in the flamelets that include differential diffusion. This influences the results and even though higher temperatures were achieved, they occurred further downstream than expected. Thirdly, it is also possible that the differential diffusion included in the flamelets is too strong for the turbulent flames in the experiment. To see if the chemical kinetic model used was the cause of some of these problems, two other chemical models have been evaluated. It was however concluded that other chemical models gave very similar results. Finally, it was noted that there were systematic differences when comparing the flamelets to the experimental data. The range covered by the experiments is larger than that covered by the FGM (at the rich side) which could also lead to underpredictions in the temperature at the nozzle. Despite the issues, the model including differential diffusion did show an improvement on the maximum flame temperature close to the nozzle compared to the other models, but there was still an error of 20% compared to an error of 30-35% in the other models.

The method used to create the PDF assumed that the progress variable and mixture fraction are statistically independent and therefore the PDF has the shape of a β -PDF. In this work it was found that the assumption of statistical independence was not correct for this flame. However, the marginal PDF still came close in shape to the β -PDF and therefore the assumption of a β -PDF was sufficiently accurate. It was however also seen that discrepancies occurred for larger values of Z which could lead to inaccuracies at the nozzle.

From this research it can be concluded that it is possible to include differential diffusion in a RANS FGM model in Fluent but several issues have to be addressed to get more reliable results. One of the main questions was if using a more elaborate chemical scheme would improve results compared to previous research by Maragkos [24] but due to these issues it is not conclusive whether using a more elaborate chemical scheme gives better results regarding the differential diffusion. The main advantage of this model compared to mod-

els used in other research is the computational time. Since computational time is linearly related to costs, it is worth investigating further.

As there is still a lot to be researched regarding the topic of modelling differential diffusion, several recommendations can be made. These recommendations have been split into different categories for a better overview

Direct extensions of this study

- The UDF in its current form did not include the calculation of the mass fraction of different species. For a better understanding of the model and why it gives peaks in the results it could be useful to have a better insight in how the species behave. It can also be interesting to see the behavior of OH as it is important for the flame structure. There are two ways to include the species. One is to expand the UDF and use the species in the simulation itself by including them into the PDF integrated table created for Fluent. The other way is to use the progress variable and mixture fraction to read the mass fraction of the species from the PDF table, as they are included.
- To get better insight in the results it can be useful to compare the variance of the progress variable and mixture fraction to the experimental data. They will need to be calculated. Appendix B explains how this possibly can be done.
- It was observed that the turbulent kinetic energy close to the nozzle was too low. Previous research has also shown that the inlet boundary conditions are complex to model and can have an influence on the simulation close to the nozzle. It is therefore recommended to see if other boundary conditions might give better results. Fluent is limited in the boundary conditions that can be applied but using a UDF is a good way to impose other boundary conditions

Other validation cases

- This research has studied a turbulent non-premixed jet flame. Due to the scope of this research no other flames have been modelled using the same approach. Using a different flame, e.g. a non-premixed helium hydrogen flame instead of the non-premixed nitrogen hydrogen flame can give new insights into the used models and the behaviour of differential diffusion. A next step from this could be to use a pre-mixed hydrogen flame in the same kind of simulation to see if it can be adapted for these kind of flames.

Other type of models and CFD software

- The literature review showed that the transported PDF is a promising model to use for modelling differential diffusion. Future research can also look into this option.
- Ansys Fluent was used in this research, but it has several limitations. The FGM created by CHEM1D also works in OpenFOAM, which might give more flexibility for development and testing of new models.

A

UDF code

```
#include "udf.h"
#include "sg_mem.h" /*necessary for scaled progress variable*/
#include "pdf_props.h"
#include "pdf_table.h"
#include "mem.h"
#include "materials.h"

/*-----DEFINITIONS size of PV_min/max table-----*/
#define nMFO 101
#define nMFVar0 11
/*-----DEFINITIONS size of independent variable table-----*/
#define nMF 101
#define nMFVar 11
#define nPV 101
#define nPVVar 11
#define sizeT 1234321

real parMFO[nMFO], parMFVar0[nMFVar0];
real parMF[nMF], parMFVar[nMFVar], parPV[nPV], parPVVar[nPVVar];

real matric_Ycb[nMFO][nMFVar0];
real matric_Ycu[nMFO][nMFVar0];

real vector_Temp[sizeT];
real vector_Cp[sizeT];
real vector_Density[sizeT];
real vector_MeanMass[sizeT];
real vector_sPV[sizeT];

DEFINE_EXECUTE_ON_LOADING(set_CV, udfCV)
{
int i,j,k,l;

for (i=0; i<nMF; i++)
parMF[i]=i*(1/(real)(nMF-1));

for (j=0; j<nMFVar; j++)
parMFVar[j]=j*(1/(real)(nMFVar-1));
```

```

for (k=0; k<nPV; k++)
parPV[k]=k*(1/(real)(nPV-1));

for (l=0; l<nPVVar; l++)
parPVVar[l]=l*(1/(real)(nPVVar-1));

for (i=0; i<nMF0; i++)
parMF0[i]=i*(1/(real)(nMF0-1));

for (j=0; j<nMFVar0; j++)
parMFVar0[j]=j*(1/(real)(nMFVar0-1));

Message0("parMF[100]=%lf, parMF[86]=%lf\n",parMF[100] ,parMF[86]);
}

DEFINE_EXECUTE_ON_LOADING(read_Ycu_b_table, udfYcmaxmin)
{
int i4, j4, k4;

FILE *rfile7, *rfile8; /*declare FILE name as pointer*/

char dummyCS[20]; /*to read a sentence*/
char dummyC; /*la traduccion de dummy es como muneco*/
int dummyI; /*la traduccion de dummy es como muneco*/

rfile7 = fopen("PVmax_table", "r"); /*open file for reading*/

fscanf(rfile7, "%s\n", dummyCS); /*read "PV_max and throw, & symbol mean to find the
                                adress of the variable*/
fscanf(rfile7, "%d\n", &dummyI); /*read "11" and throw*/
fscanf(rfile7, "%c\n\n", &dummyC); /*read "(" and throw*/

for (i4 = 0; i4 < nMFVar0; i4++)
{
fscanf(rfile7, "%d\n", &dummyI); /*read "101" and throw*/
fscanf(rfile7, "%c\n", &dummyC); /*read "(" and throw*/

for (j4 = 0; j4 < nMF0; j4++)
{
fscanf(rfile7, "%le\n", &matric_Ycb[j4][i4]); /*read "11" elements and save */
}
fscanf(rfile7, "%c\n\n\n", &dummyC); /*read ")" and throw*/

}
fscanf(rfile7, "%c\n", &dummyC); /*read ")" and throw*/
fclose(rfile7);
Message0("the Ycb[50][7]=%le\n", matric_Ycb[50][7]);

rfile8 = fopen("PVmin_table", "r"); /*open file for reading*/

fscanf(rfile8, "%s\n", dummyCS); /*read "PV_max and throw, & symbol mean to find the
                                adress of the variable*/
fscanf(rfile8, "%d\n", &dummyI); /*read "11" and throw*/
fscanf(rfile8, "%c\n\n", &dummyC); /*read "(" and throw*/

```

```

for (i4 = 0; i4 < nMFVar0; i4++)
{
fscanf(rfile8, "%d\n", &dummyI); /*read "101" and throw*/
fscanf(rfile8, "%c\n", &dummyC); /*read "(" and throw*/

for (j4 = 0; j4 < nMF0; j4++)
{
fscanf(rfile8, "%le\n", &matric_Ycu[j4][i4]); /*read "101" elements and save */
}
fscanf(rfile8, "%c\n\n", &dummyC); /*read ")" and throw*/

}
fscanf(rfile8, "%c\n", &dummyC); /*read ")" and throw*/
fclose(rfile8);
Message0("the Ycu[50][7]=%le\n", matric_Ycu[50][7]);

}

DEFINE_EXECUTE_ON_LOADING(read_Temperature_table, udfTCprhosPVmM)
{
int i, j, k, q, n;

/*vector_Temp = (real *)malloc(nMF*nMFVar*nPV*nPVVar*sizeof(real));
vector_Cp = (real *)malloc(nMF*nMFVar*nPV*nPVVar*sizeof(real));
vector_Density = (real *)malloc(nMF*nMFVar*nPV*nPVVar*sizeof(real));
vector_sPV = (real *)malloc(nMF*nMFVar*nPV*nPVVar*sizeof(real));
vector_MeanMass = (real *)malloc(nMF*nMFVar*nPV*nPVVar*sizeof(real));*/

FILE *rfile; /*declare FILE name as pointer*/

char dummyCS[20]; /*to read a sentence*/
char dummyC; /*to read a character*/
int dummyI; /*to read an integer*/

rfile = fopen("Temperature_table", "r"); /*open file for reading*/
n=0;

fscanf(rfile, "%s\n", dummyCS); /*read "Temperature_table and throw */
fscanf(rfile, "%d\n", &dummyI); /*read "11" and throw*/
fscanf(rfile, "%c\n\n", &dummyC); /*read "(" and throw*/

for (i = 0; i < nPVVar; i++)
{
fscanf(rfile, "%d\n", &dummyI); /*read "101" and throw*/
fscanf(rfile, "%c\n\n", &dummyC); /*read "(" and throw*/

for (j = 0; j < nPV; j++)
{
fscanf(rfile, "%d\n", &dummyI); /*read "11" and throw*/
fscanf(rfile, "%c\n\n", &dummyC); /*read "(" and throw*/

for (k = 0; k < nMFVar; k++)
{
fscanf(rfile, "%d\n", &dummyI); /*read "101" and throw*/
fscanf(rfile, "%c\n", &dummyC); /*read "(" and throw*/

```

```

for (q = 0; q < nMF; q++)
{
fscanf(rfile, "%le\n", &vector_Temp[n]); /*read "11" elements and save */
      n += 1;
}

fscanf(rfile, "%c\n\n\n", &dummyC); /*read ")" and throw*/

}
fscanf(rfile, "%c\n\n\n", &dummyC); /*read "(" and throw*/
}
fscanf(rfile, "%c\n\n\n", &dummyC); /*read "(" and throw*/
}
fscanf(rfile, "%c\n", &dummyC); /*read "(" and throw*/
fclose(rfile);
Message0("the vector_Temp[762903]=%le\n", vector_Temp[762903]);

rfile = fopen("Cp_table", "r"); /*open file for reading*/
n=0;

fscanf(rfile, "%s\n", dummyCS); /*read "Temperature_table and throw */
fscanf(rfile, "%d\n", &dummyI); /*read "11" and throw*/
fscanf(rfile, "%c\n\n", &dummyC); /*read "(" and throw*/

for (i = 0; i < nPVVar; i++)
{
fscanf(rfile, "%d\n", &dummyI); /*read "101" and throw*/
fscanf(rfile, "%c\n\n", &dummyC); /*read "(" and throw*/

for (j = 0; j < nPV; j++)
{
fscanf(rfile, "%d\n", &dummyI); /*read "11" and throw*/
fscanf(rfile, "%c\n\n", &dummyC); /*read "(" and throw*/

for (k = 0; k < nMFVar; k++)
{
fscanf(rfile, "%d\n", &dummyI); /*read "101" and throw*/
fscanf(rfile, "%c\n", &dummyC); /*read "(" and throw*/

for (q = 0; q < nMF; q++)
{
fscanf(rfile, "%le\n", &vector_Cp[n]); /*read "11" elements and save */
      n += 1;
}

fscanf(rfile, "%c\n\n\n", &dummyC); /*read ")" and throw*/

}
fscanf(rfile, "%c\n\n\n", &dummyC); /*read "(" and throw*/
}
fscanf(rfile, "%c\n\n\n", &dummyC); /*read "(" and throw*/
}
fscanf(rfile, "%c\n", &dummyC); /*read "(" and throw*/

```

```

fclose(rfile);
Message0("the vector_Cp[762903]=%le\n", vector_Cp[762903]);

rfile = fopen("Density_table", "r"); /*open file for reading*/
n=0;

fscanf(rfile, "%s\n", dummyCS); /*read "Temperature_table and throw */
fscanf(rfile, "%d\n", &dummyI); /*read "11" and throw*/
fscanf(rfile, "%c\n\n", &dummyC); /*read "(" and throw*/

for (i = 0; i < nPVVar; i++)
{
fscanf(rfile, "%d\n", &dummyI); /*read "101" and throw*/
fscanf(rfile, "%c\n\n", &dummyC); /*read "(" and throw*/

for (j = 0; j < nPV; j++)
{
fscanf(rfile, "%d\n", &dummyI); /*read "11" and throw*/
fscanf(rfile, "%c\n\n", &dummyC); /*read "(" and throw*/

for (k = 0; k < nMFVar; k++)
{
fscanf(rfile, "%d\n", &dummyI); /*read "101" and throw*/
fscanf(rfile, "%c\n", &dummyC); /*read "(" and throw*/

for (q = 0; q < nMF; q++)
{
fscanf(rfile, "%le\n", &vector_Density[n]); /*read "11" elements and save */
n += 1;
}

fscanf(rfile, "%c\n\n\n", &dummyC); /*read ")" and throw*/
}
fscanf(rfile, "%c\n\n\n", &dummyC); /*read "(" and throw*/
}
fscanf(rfile, "%c\n\n\n", &dummyC); /*read "(" and throw*/
}
fscanf(rfile, "%c\n", &dummyC); /*read "(" and throw*/
fclose(rfile);
Message0("the vector_Density[762903]=%le\n", vector_Density[762903]);

rfile = fopen("MeanMass_table", "r"); /*open file for reading*/
n=0;

fscanf(rfile, "%s\n", dummyCS); /*read "Temperature_table and throw */
fscanf(rfile, "%d\n", &dummyI); /*read "11" and throw*/
fscanf(rfile, "%c\n\n", &dummyC); /*read "(" and throw*/

for (i = 0; i < nPVVar; i++)
{
fscanf(rfile, "%d\n", &dummyI); /*read "101" and throw*/

```

```

fscanf(rfile, "%c\n\n", &dummyC); /*read "(" and throw*/

for (j = 0; j < nPV; j++)
{
fscanf(rfile, "%d\n", &dummyI); /*read "11" and throw*/
fscanf(rfile, "%c\n\n", &dummyC); /*read "(" and throw*/

for (k = 0; k < nMFVar; k++)
{
fscanf(rfile, "%d\n", &dummyI); /*read "101" and throw*/
fscanf(rfile, "%c\n", &dummyC); /*read "(" and throw*/

for (q = 0; q < nMF; q++)
{
fscanf(rfile, "%le\n", &vector_MeanMass[n]); /*read "11" elements and save */
n += 1;
}

fscanf(rfile, "%c\n\n\n", &dummyC); /*read ")" and throw*/

}
fscanf(rfile, "%c\n\n\n", &dummyC); /*read "(" and throw*/
}
fscanf(rfile, "%c\n\n\n", &dummyC); /*read "(" and throw*/
}
fscanf(rfile, "%c\n", &dummyC); /*read "(" and throw*/
fclose(rfile);
Message0("the vector_MeanMass[762903]=%le\n", vector_MeanMass[762903]);

rfile = fopen("SourcePV_table", "r"); /*open file for reading*/
n=0;

fscanf(rfile, "%s\n", dummyCS); /*read "Temperature_table and throw */
fscanf(rfile, "%d\n", &dummyI); /*read "11" and throw*/
fscanf(rfile, "%c\n\n", &dummyC); /*read "(" and throw*/

for (i = 0; i < nPVVar; i++)
{
fscanf(rfile, "%d\n", &dummyI); /*read "101" and throw*/
fscanf(rfile, "%c\n\n", &dummyC); /*read "(" and throw*/

for (j = 0; j < nPV; j++)
{
fscanf(rfile, "%d\n", &dummyI); /*read "11" and throw*/
fscanf(rfile, "%c\n\n", &dummyC); /*read "(" and throw*/

for (k = 0; k < nMFVar; k++)
{
fscanf(rfile, "%d\n", &dummyI); /*read "101" and throw*/
fscanf(rfile, "%c\n", &dummyC); /*read "(" and throw*/

for (q = 0; q < nMF; q++)
{
fscanf(rfile, "%le\n", &vector_sPV[n]); /*read "11" elements and save */

```

```

        n += 1;
    }

    fscanf(rfile, "%c\n\n", &dummyC); /*read ")" and throw*/
}
fscanf(rfile, "%c\n\n", &dummyC); /*read "(" and throw*/
}
fscanf(rfile, "%c\n\n", &dummyC); /*read "(" and throw*/
}
fscanf(rfile, "%c\n", &dummyC); /*read "(" and throw*/
fclose(rfile);
Message0("the vector_sPV[762903]=%le\n", vector_sPV[762903]);
}
/*****

/*****
/*          FIND INDEX for LINEAR INTERPOLATION          */
/*****

/* Utilazition: find_index(imf, &mf, parMF, nMF); */
void find_index(int i0[2], real *x0, real *x, int n)
{

/*check if index in inbounds*/
if (*x0 < x[0])
{
/*printf("Out of Lower bounds!! The number of points is %d %le %le\n", n, *x0, x[0]);*/
*x0=x[0];
i0[0] = 0;
i0[1] = 1;
return;
}
if (*x0 > x[n - 1])
{
/*printf("Out of Higher bounds!! The number of points is %d %le %le\n", n, *x0, x[n - 1]);*/
*x0=x[n-1];
i0[0] = n - 2;
i0[1] = n - 1;
return;
}

/*bisection search of index*/
int i = 0;
int w = n;
while (w > i + 1)
{
int d = (i + w) / 2;
if (*x0 < x[d])
w = d;
else
i = d;
}

i0[0] = i;
i0[1] = i + 1;

```

```

return;
}
int idx_n44D(int i, int j, int k, int q, int n3, int n4, int n5)
{
return q+n3*(k+n4*(j+n5*i));
}

int idx_n33D(int i, int j, int k, int n4, int n5)
{
return k+n4*(j+n5*i);
}

int idx_n22D(int i, int j, int n5)
{
return j+n5*i;
}

/*****
/*      LINEAR INTERPOLATION      */
*****/
real lin_interp(real x0, real x1, real x2, real y1, real y2) /*get y0*/
{
return (y2 - y1) / (x2 - x1) * (x0 - x1) + y1;
}

/* utilization Ycb = interp_matricLinear2D(imf0, ivarmf0, parMF0, parMFVar0, mf, varmf,
      matric_Ycb); */
real interp_matricLinear2D(int *i0, int *j0, real *I, real *J, real IO, real JO,
real M2D[nMF0][nMFVar0])
{
/*real M1[N10][N9][N8];*/
real M0, M1, value2D;

      M0 = lin_interp(JO, J[j0[0]], J[j0[1]], M2D[i0[0]][j0[0]], M2D[i0[0]][j0[1]]);
M1 = lin_interp(JO, J[j0[0]], J[j0[1]], M2D[i0[1]][j0[0]], M2D[i0[1]][j0[1]]);
value2D = lin_interp(IO, I[i0[0]], I[i0[1]], M0, M1);

return value2D;
}

/* utilization: prop[TEMP_UDF] = interp_matricLinear44D(icvar, ic, ivarmf, imf, parPVVar,
parPV, parMFVar, parMF, varPV, dcmean, varmf, mf, vector_sPV); */
real interp_matricLinear4D(int *i0, int *j0, int *k0, int *q0, real *I, real *J, real *K,
real *Q, real IO, real JO, real KO, real QO, real *M44D)
{

real M1[2][2][2], M2[2][2], M3[2];

real value;
int i, j, k, n1, n2;

      for (i = 0; i <= 1; i++)

```

```

{
for (j = 0; j <= 1; j++)
{
for (k = 0; k <= 1; k++)
{
n1 = idx_n44D(i0[i],j0[j],k0[k],q0[0],nMF,nMFVar,nPV);
n2 = idx_n44D(i0[i],j0[j],k0[k],q0[1],nMF,nMFVar,nPV);
M1[i][j][k] = lin_interp(Q0, Q[q0[0]], Q[q0[1]], M44D[n1], M44D[n2]);
}
M2[i][j]=lin_interp(K0, K[k0[0]], K[k0[1]], M1[i][j][0], M1[i][j][1]);
}
M3[i]=lin_interp(J0, J[j0[0]], J[j0[1]], M2[i][0], M2[i][1]);
}
value = lin_interp(I0, I[i0[0]], I[i0[1]], M3[0], M3[1]);

return value;
}

/*****
/*      Modify_PDFtable      */
*****/

DEFINE_PDF_TABLE(pdf_table, m, c, t, fmean, fvar, fmean2, fvar2, cmean, cvar, h, what, prop,
x, s_pollut)
{
real Yc_eq, Yc, Ycb, Ycu;
real dcmean, varPV, mf, varmf;

mf = fmean; /*mixture fraction*/
if ((mf>0)&(mf<1))
{
varmf = fvar/(mf*(1-mf));
}
else
{
varmf = 0;
}

int imf0[2], ivarmf0[2]; /* contains two numbers, is a range*/

/*find_index(q04, &varE0, varE4D, N7);*/
find_index(imf0, &mf, parMF0, nMF0);
find_index(ivarmf0, &varmf, parMFVar0, nMFVar0);

if (c == 333)
Message0("Step 0 of DEFINE_PDF_TABLE fmean %lf, fvar %lf, fmean2 %lf, fvar2 %lf, cmean %lf,
cvar %lf, h %lf\n", fmean, fvar, fmean2, fvar2, cmean, cvar, h);

if (NULLP(THREAD_STORAGE(t, SV_PREMIXC))) /* this means C_PREMIXC is available in memory */
{
Yc = C_PREMIXC(c,t); /*un-normalized progress variable*/

```

```

        C_UDMI(c,t,0) = Yc; /* adapt the UDM index appropriately */
    }
else /* C_PRMEMIXC not available in memory -> recover it from the UDM */
{
    Yc = C_UDMI(c,t,0); /* adapt the UDM index appropriately */
}
/*
    if (fmean >1)
Message0("mf is larger than 1 %lf, fvar %lf, fmean2 %lf, fvar2 %lf, cmean %lf,
cvar %lf, h %lf\n", fmean, fvar, fmean2, fvar2, cmean, cvar, h);
    if (fvar >1)
Message0("fvar is larger than 1 %lf, fvar %lf, fmean2 %lf, fvar2 %lf, cmean %lf,
cvar %lf, h %lf\n", fmean, fvar, fmean2, fvar2, cmean, cvar, h);
    if (cmean >1)
Message0("cmean is larger than 1 %lf, fvar %lf, fmean2 %lf, fvar2 %lf, cmean %lf,
cvar %lf, h %lf\n", fmean, fvar, fmean2, fvar2, cmean, cvar, h);
    if (cvar >1)
Message0("cvar is larger than 1 %lf, fvar %lf, fmean2 %lf, fvar2 %lf, cmean %lf,
cvar %lf, h %lf\n", fmean, fvar, fmean2, fvar2, cmean, cvar, h);
*/
    Yc_eq = Get_Yc_eq(fmean,fvar);

Ycb = interp_matricLinear2D(imf0, ivarmf0, parMF0, parMFVar0, mf, varmf, matric_Ycb);
Ycu = interp_matricLinear2D(imf0, ivarmf0, parMF0, parMFVar0, mf, varmf, matric_Ycu);

if (c == 333)
Message0("Step 1 of DEFINE_PDF_TABLE is successful, get Yc=%lf, 2D interpolated Ycb=%lf,
Ycu=%lf, at mf=%lf or %lf and varmf=%lf, the original Yc_eq is %lf\n", Yc, Ycb, Ycu, mf,
fmean, varmf, Yc_eq);

    if ((Ycb-Ycu)<1e-8)
{
dcmean=0.0;
}
else
{
dcmean=(Yc-Ycu) / (Ycb - Ycu); /*scaled-normalized progress variable==C*/
}

dcmean = MAX(MIN(dcmean, 1.0), 0.0);
/*varPV=cvar;*/
    if ((dcmean>0)&(dcmean<1))
{
    varPV = cvar/(dcmean*(1-dcmean));
}
else
{
varPV = 0;
}

```

```

if (c == 333)
Message0("Step 2 of DEFINE_PDF_TABLE is successful, Yc is scaled, dcmean=%lf at mf=%lf,
varmf=%lf\n", dcmean, mf, varmf);

int imf[2], ivarmf[2], ic[2], icvar[2];

find_index(imf, &mf, parMF, nMF);
find_index(ivarmf, &varmf, parMFVar, nMFVar);
find_index(ic, &dcmean, parPV, nPV);
find_index(icvar, &varPV, parPVVar, nPVVar);

if (c == 333)
Message0("Step 2.5 of DEFINE_PDF_TABLE is successful, find_index, imf[0]=%d, imf[1]=%d,
at mf=%lf\n", imf[0], imf[1], mf);

if NULLP(pf)
Error("Please generate or read a Fluent PDF file first\n");

if (what < 0)
{
if (dcmean>0.9999999)
{
prop[TEMP_UDF] = 0.000001;
}
else
{
prop[TEMP_UDF] = interp_matricLinear4D(icvar, ic, ivarmf, imf, parPVVar, parPV,
parMFVar, parMF, varPV, dcmean, varmf, mf, vector_sPV); /* un-normalized
progress variable source term*/
}
if (c == 333)
{
Message0("Step 3 of DEFINE_PDF_TABLE is successful,source term of progress variable is
interpolated sPV= %lf 1/s\n", prop[TEMP_UDF]);
Message0("at ic[0]=%d, ic[1]=%d, imf[0]=%d, imf[1]=%d, varPV=%lf, dcmean=%lf, varmf=%lf,
mf=%lf\n", ic[0], ic[1], imf[0], imf[1], varPV, dcmean, varmf, mf);
}
}
else if (what == 1)
{
prop[TEMP_UDF] = interp_matricLinear4D(icvar, ic, ivarmf, imf, parPVVar, parPV, parMFVar,
parMF, varPV, dcmean, varmf, mf, vector_Temp);
prop[CP_UDF] = interp_matricLinear4D(icvar, ic, ivarmf, imf, parPVVar, parPV, parMFVar,
parMF, varPV, dcmean, varmf, mf, vector_Cp);
prop[DEN_UDF] = interp_matricLinear4D(icvar, ic, ivarmf, imf, parPVVar, parPV, parMFVar,
parMF, varPV, dcmean, varmf, mf, vector_Density);
prop[MOL_WT_MIX_UDF] = interp_matricLinear4D(icvar, ic, ivarmf, imf, parPVVar, parPV,
parMFVar, parMF, varPV, dcmean, varmf, mf, vector_MeanMass);
if (c == 333)
{
Message0("Step 3 of DEFINE_PDF_TABLE is successful,temperature=%lf K, Cp=%lf J/kgK,
Density=%lf kg/m3, MeanMass=%lf kg/kmol\n", prop[TEMP_UDF], prop[CP_UDF], prop[DEN_UDF],

```

```
prop[MOL_WT_MIX_UDF]);
    Message0("at ic[0]=%d, ic[1]=%d, imf[0]=%d, imf[1]=%d, varPV=%lf, dcmean=%lf,
    varmf=%lf, mf=%lf\n", ic[0], ic[1], imf[0], imf[1], varPV, dcmean, varmf, mf);
}
}
}
```

B

Relation between variance of unscaled and scaled progress variable

In FGM for non-premixed and partially premixed combustion the independent variables are mixture fraction and progress variable. For tabulation purposes the scaled progress variable is introduced. It is defined by:

$$c = \frac{Y_c - Y_{c\min}}{Y_{c\max} - Y_{c\min}} \quad (\text{B.1})$$

Here “min” and “max” refer to the minimal value and maximal value of unscaled progress variable. These values can be depending on the mixture fraction. In the case of hydrogen flames a good choice of unscaled progress variable is H2O mass fraction. In the case the oxidiser does not contain any H2O its minimal value is 0 and the scaled progress variable then becomes:

$$c = \frac{Y_c}{Y_{c\max}(Z)} \quad (\text{B.2})$$

The relations between the independent variables Z and c and other thermodynamic variables are stored in the FGM table.

In turbulent flow the mixture fraction and the progress variable are fluctuating and in the model this is described using their probability density function. Density weighted mean properties of any thermodynamic quantity that can be included in the table can then be calculated from:

$$\tilde{Y}_k = \int_0^1 \int_0^1 Y_k^{fgm}(z, c) \tilde{P}_{Zc}(z, c) dz dc \quad (\text{B.3})$$

Making the assumption that the mixture fraction and the scaled progress variable are statistically independent the joint PDF reduces to the product of the marginal PDF of mixture fraction and the marginal PDF of scaled progress variable.

$$\tilde{Y}_k = \int_0^1 \int_0^1 Y_k^{fgm}(z, c) \tilde{P}_Z(z) \tilde{P}_c(c) dz dc \quad (\text{B.4})$$

A standard approach is to make the assumption that both marginal PDFs take the form of a beta-function. This mathematical function is depending on two parameters, that can be related to the mean and variance. The model equations for mean and variance of mixture fraction and unscaled progress variable are given in the section at the end of this appendix.

In order to be able to calculate mean values it is necessary to obtain the mean and variance of scaled progress variable (appearing in the PDF) from the mean and variance of unscaled progress variable. When mixture fraction and unscaled progress variable are statistically independent these relations are:

$$\tilde{Y}_c = \tilde{c} \tilde{Y}_{c \max} \quad (\text{B.5})$$

$$\widetilde{Y_c'^2} = (\tilde{c}^2 - \tilde{c}^2) \widetilde{Y_{c \max}^2} + \left(\widetilde{Y_{c \max}^2} - \widetilde{Y_{c \max}}^2 \right) \tilde{c}^2 \quad (\text{B.6})$$

$$\widetilde{Y_c'^2} = (\tilde{c}'^2) \widetilde{Y_{c \max}^2} + \left(\widetilde{Y_{c \max}^2} \right) \tilde{c}^2 \quad (\text{B.7})$$

Note that the mean values of maximal unscaled progress variable and the square of the maximal unscaled progress variable can be obtained from:

$$\tilde{Y}_{c \max} = \int_0^1 Y_{c \max}(z) \tilde{P}_Z(z) dz \quad (\text{B.8})$$

$$\widetilde{Y_{c \max}^2} = \int_0^1 Y_{c \max}^2(z) \tilde{P}_Z(z) dz \quad (\text{B.9})$$

use these equations the maximum of unscaled progress variable must be tabulated and the averaging formula has to be applied.

Things become much simpler if the average of maximum unscaled progress variable would be the same as the unscaled progress variable evaluated at the average mixture fraction, i.e. of the following equations hold:

$$\tilde{Y}_{c \max} = Y_{c \max}(\tilde{Z}) \quad (\text{B.10})$$

$$\widetilde{Y_{c \max}^2} = Y_{c \max}^2(\tilde{Z}) \quad (\text{B.11})$$

In general these equations do not hold, but using it as a first approximation the relation between the variances simplifies to an equation that, for a given value of mean mixture fraction, provides a direct relation between variance of scaled and unscaled progress variable:

$$\tilde{Y}_c = \tilde{c} Y_{c \max}(\tilde{Z}) \quad (\text{B.12})$$

$$\widetilde{Y_c^2} = (\tilde{c}'^2) Y_{c \max}^2(\tilde{Z}) \quad (\text{B.13})$$

Bibliography

- [1] I.M. Aksit and J.B. Moss. A hybrid scalar model for sooting turbulent flames. *Combustion and Flame*, 145:231–244, 2006.
- [2] Ansys. Lecture 7: Turbulence modeling, introduction to Ansys Fluent, 2014.
- [3] Ansys Fluent. Theory guide for Fluent 19, 2019.
- [4] C.D. Argyropoulos and N.C. Markatos. Recent advances on the numerical modelling of turbulent flows. *Applied Mathematical Modelling*, 39:693–732, 2015.
- [5] M.P. Burke, M. Chaos, Y. Ju, F.L. Dryer, and S.J. Klippenstein. Comprehensive H₂/O₂ kinetic model for high-pressure combustion. *International Journal of Chemical Kinetics*, 44:444–474, 2012.
- [6] P.M. Burke, M. Chaos, Y. Ju, F.L. Dryer, and S.J. Klippenstein. Comprehensive h₂/o₂ kinetic model for high-pressure combustion. *International Journal of Chemical Kinetics*, 44:444–474, 2012.
- [7] O.R. Darbyshire and N. Swaminathan. A presumed joint pdf model for turbulent combustion with varying equivalence ratio. *Combustion Science and Technology*, 184:2036–2067, 2012.
- [8] J.A.M. de Swart, R.J.M. Bastiaans, J.A. van Oijen, L.P.H. de Goey, and R.S. Cant. Inclusion of preferential diffusion in simulations of premixed combustion of hydrogen/methane mixtures with Flamelet Generated Manifolds. *Flow Turbulence Combustion*, 85:473–511, 2010.
- [9] J.L. Devore. *Probability and Statistics for Engineering and the Sciences*. Brooks/Cole, 8th edition, 2010.
- [10] N.A.K Doan, N. Swaminathan, and Y. Minamoto. Dns of mild combustion with mixture fraction variations. *Combustion and Flame*, 189:173 – 189, 2018.
- [11] A. Donini, R.J.M. Bastiaans, J.A. Van Oijen, and L.P.H. De Goey. Differential diffusion effects inclusion with flamelet generated manifold for the modeling of stratified premixed cooled flames. *Proceedings of the Combustion Institute*, 35:831–837, 2015.
- [12] P.M. Doran. *Bioprocess Engineering Principles*. Academic Press, 2nd edition, 2013.
- [13] A. D’Ausilio, I. Stankovic, and B. Merci. Numerical study on the importance of the turbulent inlet boundary condition and differential diffusion in a turbulent H₂/N₂/air jet diffusion flame. *Combustion Science and Technology*, 191:109–125, 2019.
- [14] T. Echehki and E. Mastorakas. *Turbulent Combustion Modeling*. Springer, 1st edition, 2011.
- [15] T. Echehki, A.R. Kerstein, T.D. Dreeben, and J. Chen. ‘One-Dimensional Turbulence’ simulation of turbulent jet diffusion flames: model formulation and illustrative applications. *The Combustion Institute*, 125:1083–1105, 2001.
- [16] M. Fishedick, J. Adolf, K. Arnold, A. Pastowski, D. Schüwer, C.H. Balzer, J. Louis, and U. Schabla. Energy of the future: Sustainable mobility through Fuel Cells and H₂. Technical report, Shell and Wuppertal Institute for Climate, Energy and Environment, 2017.
- [17] H. Forkel and J. Janicka. Large-Eddy Simulation of a turbulent hydrogen diffusion flame. *Flow, Turbulence and Combustion*, 65:163–175, 2000.
- [18] Y. Gao and N. Chakraborty. Modeling of Lewis number dependence of scalar dissipation rate transport for Large Eddy Simulations of turbulent premixed combustion. *Numerical Heat Transfer; Part A: Applications*, 69:1201–1222, 2016.

- [19] W. Han, V. Raman, and Z. Chen. LES/PDF modeling of autoignition in a lifted turbulent flame: Analysis of flame sensitivity to differential diffusion and scalar mixing time-scale. *Combustion and Flame*, 171: 69–86, 2016.
- [20] A. Kempf, A. Sadiki, and J. Janicka. Prediction of finite chemistry effects using Large Eddy Simulation. *Proceedings of the Combustion Institute*, 29:1979–1985, 2002.
- [21] C. Kleinhardt. H3. URL https://www.dlr.de/vt/en/desktopdefault.aspx/tabid-3067/4635_read-6728/. Last accessed: 24-6-2020.
- [22] J. Li, Z. Zhao, A. Kazakov, and F.L. Dryer. An updated comprehensive kinetic model of hydrogen combustion. *International Journal of Chemical Kinetics*, 36:566–575, 2004.
- [23] M.C. Ma and C.B. Devaud. A Conditional Moment Closure (CMC) formulation including differential diffusion applied to a non-premixed hydrogen-air flame. *Combustion and Flame*, 162:144–158, 2015.
- [24] G. Maragkos, P. Rauwoens, and B. Merci. Assessment of a methodology to include differential diffusion in numerical simulations of a turbulent flame. *International Journal of Hydrogen Energy*, 40:1212–1228, 2015.
- [25] W. Meier, S. Prucker, M.H. Cao, and W. Stricker. Characterization of turbulent H₂/N₂/air jet diffusion flames by single-pulse spontaneous Raman scattering. *Combustion Science and Technology*, 118:293–312, 1996.
- [26] W. Meier, A.O. Vydrov, V. Bergmann, and W. Stricker. Simultaneous Raman/LIF measurements of major species and NO in turbulent H₂/air diffusion flames. *Applied Physics B: Lasers and Optics*, 63:79–90, 1996.
- [27] T. Nagy, C. Olm, I.G. Zsély, T. Varga, Pálvölgyi R., G. Valkó, É. Vincze, and T. Turányi. Optimisation of a hydrogen combustion mechanism. *Proceedings of the European Combustion Meeting*.
- [28] B. Naud, R. Novella, J.M. Pastor, and J.F. Winklinger. RANS modelling of a lifted H₂/N₂ flame using an unsteady flamelet progress variable approach with presumed PDF. *Combustion and flame*, 162:893–906, 2015.
- [29] A. Neuber, G. Krieger, M. Tacke, E. Hassel, and J. Janicka. Finite rate chemistry and NO molefraction in non-premixed turbulent flames. *Combustion and Flame*, 113:198–211, 1998.
- [30] F.T.M. Nieuwstadt, B.J. Boersma, and J. Westerweel. *Turbulence: Introduction to Theory and Applications of Turbulent Flows*. Springer, 2016.
- [31] A.A.V. Perpignan, A. Gangoli Rao, and D.J.E.M. Roekaerts. Flameless combustion and its potential towards gas turbines. *Progress in Energy and Combustion Science*, 69:28–62, 2018.
- [32] D.G. Pfuderer, A.A. Neuber, G. Fruchtel, E.P. Hassel, and J. Janicka. Turbulence Modulation in Jet Diffusion Flames: Modeling and Experiments. *Combustion and Flame*, 106:301–317, 1996.
- [33] H. Pitsch. Unsteady Flamelet Modeling of Differential Diffusion in Turbulent Jet Diffusion Flames. *Combustion and Flame*, 123:358–374, 2000.
- [34] H. Pitsch, M. Chen, and N. Peters. Unsteady Flamelet Modeling of Turbulent Hydrogen-Air Diffusion Flames. *The Combustion Institute Symposium*, 27:1057–1064, 1998.
- [35] T. Poinso and D. Veynante. *Theoretical and Numerical Combustion*. Edwards, 3rd edition, 2001.
- [36] S.B. Pope. An explanation of the turbulent round-jet/plane-jet anomaly. *AAIA Journal*, 16:279–281, 1978.
- [37] W.J.S. Ramaekers, B.A. Albrecht, J.A. van Oijen, L.P.H. de Goey, and R.L.G.M. Eggels. The application of Flamelet Generated Manifolds in turbulent partially-premixed flames. In *Proceedings of the Fluent Benelux User Group Meeting, 6-7 October 2005, Wavre, Belgium*, 2005.

- [38] B. Ranganath and T. Echehki. One-Dimensional Turbulence-based closure for turbulent non-premixed flames. *Progress in Computational Fluid Dynamics*, 6:409–418, 2006.
- [39] M. Ren, S. Wang, and D. Roekaerts. Numerical study of the counterflow diffusion flames of methanol hydrothermal combustion: The real-fluid effects and flamelet analysis. *The Journal of Supercritical Fluids*, 152:104552, 2019.
- [40] M.W. Renfro, A. Chaturvedy, G.B. King, N.M. Laurendeau, A. Kempf, A. Dreizler, and J. Janicka. Comparison of OH time-series measurements and large-eddy simulations in hydrogen jet flames. *Combustion and Flame*, 139:142–151, 2004.
- [41] E.S. Richardson and J.H. Chen. Application of PDF mixing models to premixed flames with differential diffusion. *Combustion and Flame*, 159:2398–2414, 2012.
- [42] N. Romero-Anton, X. Huang, H. Bao, Martin-Eskuderom K., E. Salazar-Herran, and D. Roekaerts. New extended eddy dissipation concent model for flameless combustion in furnaces. *Combustion and flame*, 220:49–62, 2020.
- [43] J.A. van Oijen, A. Donini, R.J.M. Bastiaans, J.H.M. ten Thije Boonkkamp, and L.P.H. de Goey. State-of-the-art in premixed combustion modeling using flamelet generated manifolds. *Progress in Energy and Combustion*, 57:30–74, 2016.
- [44] H. Wang. Consistent flamelet modeling of differential molecular diffusion for turbulent non-premixed flames. *Physics of Fluids*, 28:035102, 2016.
- [45] J. Warnatz, U. Maas, and R.W. Dibble. *Combustion: physical and chemical fundamentals, modeling and simulation, experiments, pollutant formation*. Springer, 4th edition, 2006.
- [46] H. Zhou, T. Yang, and Z. Ren. Differential diffusion modeling in LES/FDF simulations of turbulent flames. *AIAA Journal*, 57:No. 8, 2019.